Response to the referees' and short comments

Dear referees,

We are very grateful for your valuable comments. Please find our detailed responses below, in italics. Revisions to the manuscript are highlighted in yellow in the "revised manuscript" file, attached. For convenience, we also attach a version of the manuscript with changes incorporated. We hope you are satisfied with our revisions, and we are happy to receive further feedback.

With our best regards,

Xuanmei Fan and co-authors

Referee #1 – A. Strom

Comment #1

Dear Authors,

Thank you for interesting paper. It can be accepted after minor correction in Table 3. It seems that V_{total} is in m^3 not in millions m^3 (otherwise values are too large). I think that you can avoid separating of 3 orders by commas.

Response #1

Dear prof. Strom,

We thank you for taking the time to review our manuscript and we sincerely appreciate your positive review. Table 3 has been corrected according to your comment.

Referee #2 – Anonymous

Comment #1

The authors describe two datasets of post-earthquake geohazard events that were collected after the 2008 Wenchuan earthquake. One if a multi-temporal landslide inventory of the area along the Minyang river near the epicenter, and the other a database of debris flow watersheds and debris flow events. The authors have published this data and made it freely available to other researchers, which is a very important step towards an improved understanding of post-earthquake geohazards.

Response #1

Dear referee,

We thank you for taking the time to review our manuscript, and for your valuable and constructive comments. Please find our detailed reply below. For further information about the contents uploaded in the repository, please find a copy of the word document named "readme.doc" (also placed it in the repository) at the end of this file.

Comment #2

Initiatives for collecting coseismic landslide inventories have been recently undertaken by Tanyas et al (2017) and Schmidt et al. (2017) who established a web based repository of landslide inventories (https://pubs.usgs.gov/ds/1064/ds1064.pdf and https://www.sciencebase.gov/catalog/item/583f4114e4b04fc80e3c4a1a. The current inventory could also have been submitted to this platform so that also post earthquake inventories can be shared. Nevertheless, the sharing of this inventory is important.

Response #2

We are aware and strongly support the initiative by Schmitt et al. However, our work concerns post-earthquake inventories. As such, it does not strictly fit in the scope of the database compiled by Schmidt et al., which is in fact entitled "An Open Repository of Earthquake-

Triggered Ground-Failure Inventories". With the present work, in fact, we wish to promote the sharing and collecting of datasets that concern the post-earthquake geohazards and their spatial and temporal evolution. We chose Zenodo (created by OpenAIRE within EU's programme Horizon 2020, and hosted at CERN) to reposit our dataset, and we chose this open-access journal (ESSD) to present our work and encourage other researchers to share theirs.

Comment #3

It is another issue, however, whether this merits a publication which is mostly descriptive, and repetitive. The description of the data set for post-earthquake landslide and analysis results were presented in an earlier paper of the authors in Landslides (doi: 10.1007/s10346-018-1054-5, 2018a) and the debris flow dataset was also presented in Tang and Van Westen (2018) (Tang, C., & van Westen, C. J, 2018, Atlas of Wenchuan-Earthquake Geohazards: Analysis of co-seismic and postseismic Geohazards in the area affected by the 2008 Wenchuan Earthquake. Science Press). Why was the dataset not attached to the earlier publication in Landslides? This paper contains relevant limited new information.

Response #3

As the referee recognised, only results from the dataset of post-earthquake landslides have been presented in an earlier paper, where some of the implications that can be drawn from it have been discussed. However, the dataset has been refined and updated since then, and is therefore ready to be published in an open-access repository only now. After the submission of the paper, the latest imagery of the area is available, so we also updated our post-seismic landslide inventory for the years 2017 and 2018.

Regarding the dataset of debris flows, this is the first time that such a large multitemporal dataset is published and described. As the co-author (a contributor) of the Atlas, I can guarantee there is no such comprehensive debris flow database published in the Atlas. In the Atlas, only some case studies and results from specific areas are reported with multi-temporal information, as shown in a descriptive table that includes about 90 debris flows (as shown in Fig 1).

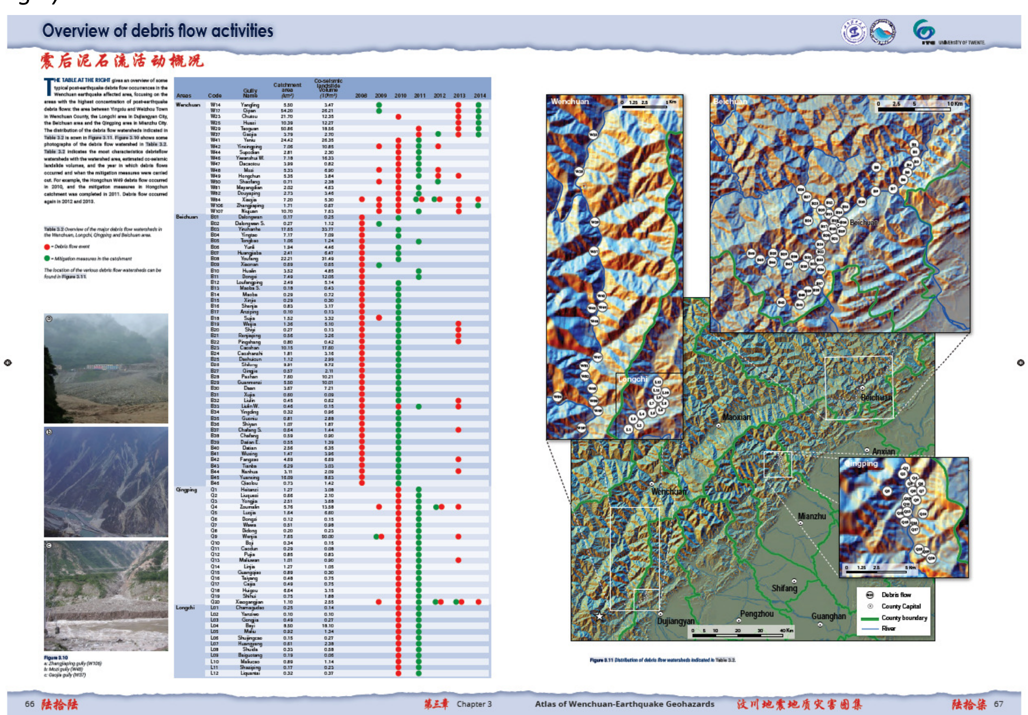

Figure 1: The debris flow information from Atlas (Tang and van Westen): page 66-67. The table lists 92 debris flows mainly from four regions (Wenchuan, Beichuan, Qingping and Longchi)

and includes only the rough location, year of occurrence and an estimation of the total amount of coseismic landslide volume.

*Our dataset covers a much large area and a longer time frame than that used by Tang and van Westen in their Atlas. It includes **527 post-seismic debris flow events**, almost 6 times more than the list in the Atlas. Most importantly, we presented detailed information of each debris flow event, such as the accurate occurrence time, source and deposition volume, rainfall information of surrounding rain gauges etc. The database are both in Excel format (Figure 2) and geo-referenced GIS shp file format with detailed attribute table (Figure 3).*

Gully name	DF_ID	CID	Latitude	Longitude	Year	Month	Day	Time(24h)	T_Comment	Source volume (m^3)	Depo_vol (m^3)	List of RG_ID	Monitoring(Y/N)	Number of Dams	Reference of Data source
Xiangzhangshu 1#/Baiguoping	203	P5	103.868	31.316	2008	5	18	-	-	21600	1850	44	N	-	Ma et al. 2011; Wang et al. 2014
Xiangzhangshu 1#/Baiguoping	204	P5	103.868	31.316	2012	8	18	00:30	Initiation	183900	-	44	N	-	Huang et al. 2013
Xiangzhangshu 1#/Baiguoping	205	P5	103.868	31.316	2008	7	-	-	-	-	1650	-	N	-	Wang et al. 2014
Guanzi	206	P6	103.873	31.3248	2012	8	18	00:30	Initiation	5394700	-	44	N	-	Huang et al. 2013
Banjie	207	P7	103.876	31.328199	2012	8	18	00:30	Initiation	894600	-	44	N	-	Huang et al. 2013
Haihuiqiao 1#/Gaojiazi	208	P8	103.88	31.337601	2010	8	18	-	-	-	-	44	N	-	Ma et al. 2011
Haihuiqiao 1#/Gaojiazi	209	P8	103.88	31.337601	2012	8	18	00:30	Initiation	2570000	250000	44	N	-	Huang et al. 2013; Yu et al. 2014
Tongchangpo	210	P9	103.781	31.2332	2008	7	21	-	-	70700	3000	-	N	2	Wang et al. 2016b
Dianzhan	211	M1	104.1056	31.575826	2010	8	13	01:00	Initiation	21000	1000	64 , 65 , 43	N	1	Su et al. (2011)
Heitanzi	212	M1	104.1062	31.57641	2010	8	13	01:30	Initiation	-	12600	64 , 65 , 43	N	1	Tang et al. (2012a)
Bojiyan	213	M10	104.1078	31.553912	2010	8	13	01:00	Initiation	27000	7000	64 , 65 , 43 , 62	N	-	Su et al. (2011) ; Ni et al. (2011)
Boji	214	M10	104.1069	31.55379	2010	8	13	01:30	Initiation	-	3600	64 , 65 , 43 , 62	N	-	Tang et al. (2012a)
Caodun	215	M11	104.1094	31.550998	2010	8	13	01:30	Initiation	-	15000	64 , 43 , 65 , 62 , 57	N	-	Tang et al. (2012a)
Wangjiashan	216	M12	104.1057	31.545862	2010	8	13	01:00	Initiation	12500	2500	64 , 65 , 43 , 62	N	1	Ni et al. (2011)
Pujia	217	M12	104.106	31.546273	2010	8	13	01:30	Initiation	-	5800	64 , 65 , 43 , 62	N	1	Tang et al. (2012a)
Maliuwan	218	M13	104.1086	31.543635	2010	8	13	01:30	Initiation	-	24000	64 , 65 , 43 , 62 , 57	N	-	Tang et al. (2012a)
Yingjia	219	M14	104.1146	31.542891	2010	8	13	01:00	Initiation	50000	8000	64 , 43 , 62 , 57 , 65 , 61	N	1	Su et al. (2011)
Linjia	220	M14	104.1149	31.542657	2010	8	13	01:30	Initiation	-	39600	64 , 43 , 62 , 57 , 65 , 61	N	-	Tang et al. (2012a)
Guangqiao	221	M15	104.1101	31.53687	2010	8	13	01:30	Initiation	-	27800	64 , 43 , 62 , 65 , 57	N	1	Tang et al. (2012a)
Taiyang	222	M16	104.1166	31.535455	2010	8	13	01:00	Initiation	5000	20000	64 , 43 , 62 , 57 , 61 , 65	N	1	Su et al. (2011)
Taiyang	223	M16	104.1148	31.535252	2010	8	13	01:30	Initiation	-	127800	64 , 43 , 62 , 57 , 65 , 61	N	-	Tang et al. (2012a)
Caijia	224	M17	104.1149	31.53111	2010	8	13	01:30	Initiation	-	60400	64 , 43 , 62 , 57 , 61 , 65	N	-	Tang et al. (2012a)
Huigou	225	M18	104.1178	31.51293	2010	8	13	01:30	Initiation	-	285100	64 , 62 , 43 , 57 , 61	N	-	Tang et al. (2012a)
Chengqiangya	226	M19	104.1247	31.50921	2010	8	13	01:00	Initiation	24000	4000	64 , 62 , 43 , 57 , 61	N	-	Su et al. (2011)
Shihui	227	M19	104.1249	31.509404	2010	8	13	01:30	Initiation	-	84200	64 , 43 , 62 , 57 , 61	N	-	Tang et al. (2012a)
liubaizi	228	M2	104.1072	31.572222	2010	8	13	01:00	Initiation	22500	2500	64 , 65 , 43	N	1	Su et al. (2011)
Liuquezi	229	M2	104.1062	31.57295	2010	8	13	01:30	Initiation	-	27100	64 , 65 , 43	N	-	Tang et al. (2012a)
Changtan	230	M20	104.1275	31.503889	2010	8	17	-	-	-	-	64 , 62 , 43 , 57 , 61	N	-	http://news.163.com/10/0818/14/6ECH82HN000146BD.html
Xiaogangjian	231	M20	104.1294	31.503333	2014	6	4	-	-	-	10000	62 , 43 , 64 , 57 , 61	N	9	http://scnews.newssc.org/system/20140604/000391154.html
Changtan	232	M20	104.1275	31.503889	2010	8	13	01:00	Initiation	-	300000	64 , 62 , 43 , 57 , 61	N	-	Su et al. (2011)
Xiaogangjian	233	M20	104.1294	31.504025	2010	8	13	01:30	Initiation	-	290200	62 , 43 , 64 , 57 , 61	N	-	Tang et al. (2012a)
Xiaogangjian	234	M20	104.1294	31.503333	2010	8	18	-	-	-	-	62 , 43 , 64 , 57 , 61	N	-	Yang et al. (2012)

Figure 2: A screenshot of our debris flow database includes 527 debris flows events with detailed information (Excel format, can be download from https://doi.org/10.5281/zenodo.1405489)

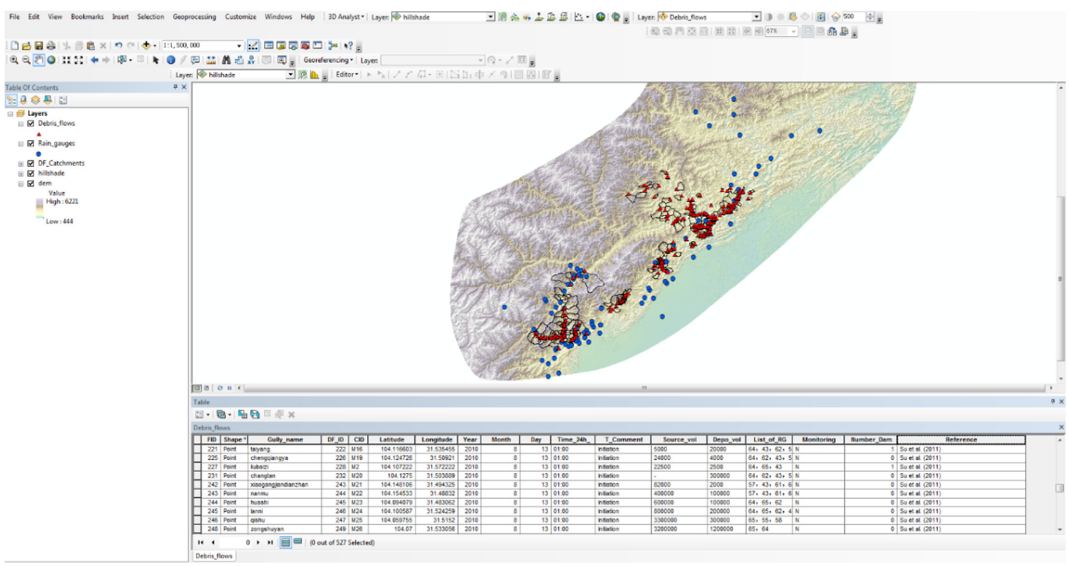

Figure 3: A screenshot of the GIS shp file with detailed attributes (can be download from https://doi.org/10.5281/zenodo.1405489)

Regarding the descriptive nature of the manuscript, this is actually intentional. Our aim is to present the datasets, their coverage, the methods for their preparation, and to provide descriptive statistics. We wish in fact to provide the community with the source data, and with the tools to understand them and evaluate their reliability and value. We believe that detailed interpretations or discussions of our data also would fall beyond the scope for which this article has been thought, and be more appropriate for a different editorial context. We have read the journal guidelines and inquired the editors during the preparation of the manuscript and dataset (i.e. prior to submission), and we understand the scope of the journal is for the publication of articles on original research data (sets).

Some choices in the selection of data also are, on purpose, as inclusive as possible. This is the case, for instance, of the selection of the rain gauges that are coupled to a debris flow event: we chose a distance which is large enough to ensure that all the relevant rain gauges are included (given the high variability of rainfall in the mountain area) and we avoided on purpose to make arbitrary choices (e.g. by selecting only the closest rain gauge to the debris flow event) which would make the dataset less usable and flexible. These choices remain up to the users of the datasets, who can thus make them according to their purpose and justify them.

Comment #4

Methodologically, the analysis of the post-earthquake landslides is based on an earlier paper by Tang et al. 2016 (https://doi.org/10.5194/nhess-16-2641-2016). Also because they mapped almost the same area. The existing study has extended this area a bit but followed basically the same approach and classification method.

Response #4

We thank the reviewer for the comments, but we would like to address the following issues that the reviewer may have overlooked. Firstly, the area we investigated is much larger than that covered by Tang et al. (it is almost three times larger, please see Figure 4 below). Secondly, the method has a key difference. In fact, differently from earlier works (Tang et al. 2016), where the same coseismic landslide polygon was used in the following years to evaluate, qualitatively, the level of activity in the attribute table (Figure 5-a), we quantified at each time changes of the level of activity based on new, actual polygon-mapping of remobilised areas (Figure 5-b). We have now pointed out this better in the revised manuscript. Note that <u>only for ease of visualization and to facilitate comparisons</u>, we retained the same definitions of the activity levels (A0-A3) as those given by Tang et al. However, it is clear that their meaning is not the same, because we actually re-mapped and thus quantified the remobilized areas on each imagery rather than providing a qualitative estimation of the activity level.

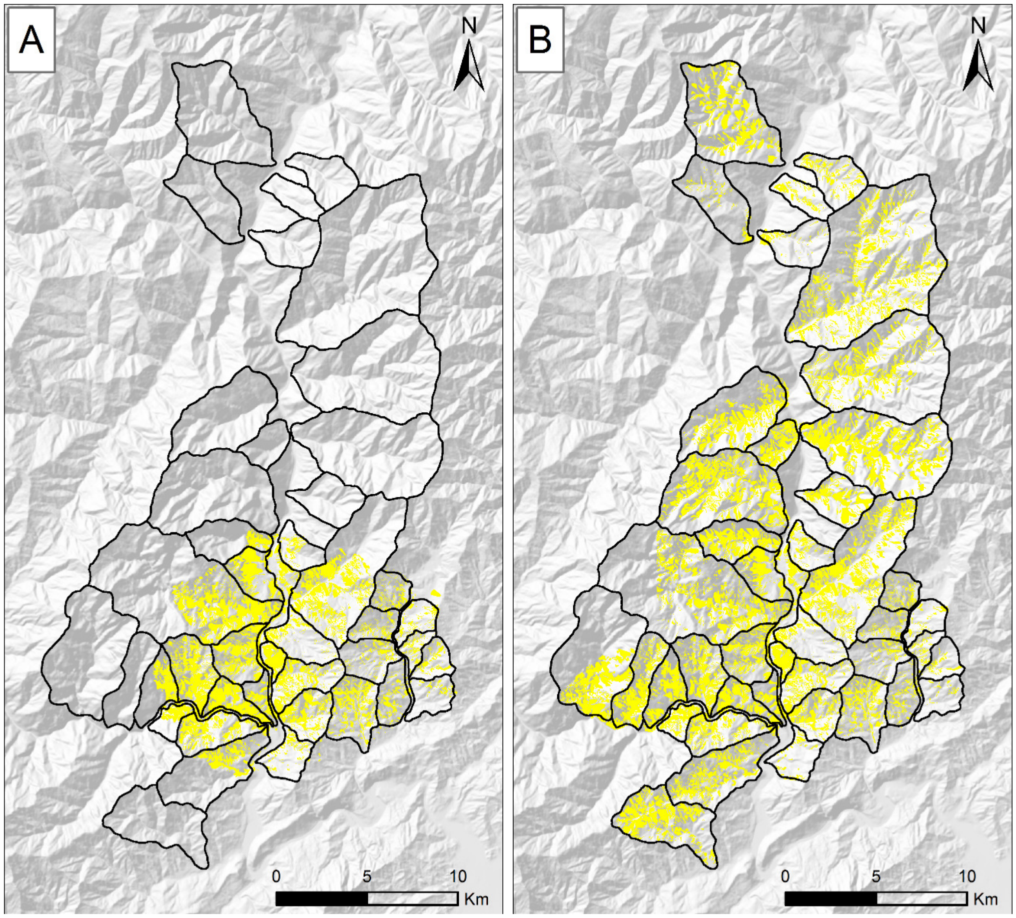

Figure 4: co-seismic mapping performed by Tang et al. (2016) (A) and by the authors of the manuscript (B).

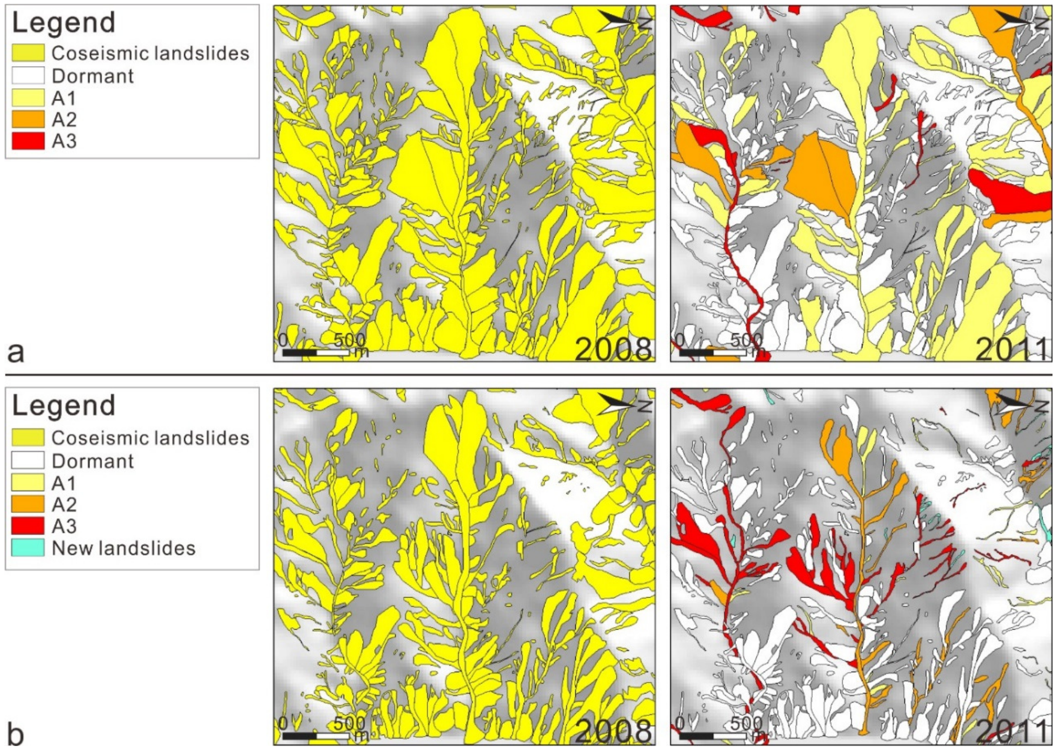

Figure 5: coseismic and post-seismic inventory for year 2011 performed by Tang et al. (2016) (a). In 2011, the same coseismic landslide polygons are used and the activity level is stored in the table of attributes. Conversely, in our multi-temporal inventory (b), we delineated the remobilised area.

Comment #5

If the paper is about the dataset, then it would be better to focus more on a quantitative analysis of the dataset. For instance by quantitatively analyzing the completeness and accuracy, and by comparing the dataset with other data sets for the same area (e.g. there are several co-seismic and postseismic landslide inventories made for this area).

Response #5

*We thank the reviewer for the comment. For the coseismic inventory, as there are some other inventories available, we are able to compare our inventory with other polygon-based inventories, such as Dai et al. (2011); Xu et al. (2014) and Tang et al. (2016), **please see the new section3.1.4 in the revised manuscript**. For the post-seismic inventory, our dataset is the first multi-temporal dataset that is freely downloadable from an open repository. Unfortunately, there are no other multi-temporal datasets that cover the same area. Thus, we are unable to make a quantitative spatial analysis of our dataset for completeness and accuracy. Only qualitative comparisons could be made, by comparing our maps to those produced by other authors.*

Comment #6

The debris flow watershed database should also contain information on when and what was carried out in the watershed in terms of mitigation measures. A real analysis of debris flow occurrence, rainfall, and treatment of the watersheds is basically missing.

Response #6

Most of the mitigation measures carried out in the watersheds are landslide dams which retain the material during storms. In the Dataset 2 (see the repository:

https://doi.org/10.5281/zenodo.1405489*), we specified the number of dams present in each catchment. As pointed by the referee, it would be very interesting to know when the dams were built. Most of check dams were built in 2011-2012. Unfortunately, detailed date information for each dam is missing.*

Comment #7

What is the relationship between the two datasets? Are the events mapped as debris flows in the landslide dataset the same as in the debris flow dataset?

Response #7

In Dataset1 we have two type of debris flows: hillslope debris flows, which are found along the hillslopes and channelized debris flows, which are found into small channels. Then, the channelized deposits are large amounts of accumulated debris, found in the main channels were clear remobilisations could not be identified. Furthermore, the source of these materials is not known as they come from different debris flows and slides (debris and rock slides, debris and rock falls) that occurred upstream. Conversely, the debris flows reported in Dataset2 are big events that reached or approached the outlet of the catchment affecting facilities and/or the population. In such case, the material can come from the slides, hillslope and channelized debris flow and, mainly, form the existing channel deposits material, all of them presented in Dataset1. Dataset2 events have been reported by several authors (see references) but they were not systematically mapped, and this is why they have been represented as points. Differently from events in Dataset1, Dataset2 events in some cases include the information about the day and time of the occurrence. Therefore, these events can be correlated with the triggering rainfalls, included also in the Dataset2, to perform analysis of magnitude-frequency (temporal) for a later application of early warning systems, for instance. Nevertheless, these Dataset2 does not allow to carry out spatial analyses about the source material in terms of controlling terrain factors, or spatial and temporal evolution of instabilities; such analysis have to be carried out using the Dataset1. This has been clarified in the text.

Comment #8

The paper has a bit too many references for not being a review paper. In my view the number of references could be reduced a bit, only using the really relevant ones.

Response #8

We deleted some non-key or redundant references.

Comment #9

Specific comments: 1/16: event should be events

Response #9

Corrected.

Comment #10

2/23-24: landslide inventories are important for more reasons than indicated here. This could be further elaborated

Response #10

We re-elaborated this part in the manuscript.

Comment #11

2/26-27: “several” seems it of an understatement. This work contains over 44 inventories.

Response #11

We changed to “many”.

Comment #12

2/33: examples of references are also from other earthquakes, like Kashmir (Saba et al).

Response #12

In fact, we write "after major earthquakes, particularly after …", meaning that Chi-Chi and Wenchuan are the most important, i.e. for which the most extensive research has been carried out, but not the only ones.

Comment #13

4/10: how realistic are these empirical area-volume relationships when you compare them for your study area. This would be interesting in terms of the dataset, and the resulting conclusions that can be drawn from them. If you take the data from Parker et al (2011) and your own dataset and compare the area-volume relationships, they might show large differences.

Response #13

Both Parker et al. and Xu et al. employed their relationships to estimate coseismic landslide volumes after the Wenchuan earthquake. Nevertheless, their results show large variability because of how the relationships were calibrated, hence the large difference between the estimations that we reported (0.8 and 1.5 billion m^3). A discussion on the reliability of these area-volume relationships is beyond the scope of this work, but can be found in the supplementary material (online resource n. 2) attached to Fan et al. (2018c). We included a reference to this in the revised manuscript.

Comment #14

6/1-6: Why did you not use different DEMs before and after the earthquake, given that the earthquake produced large differences in elevation?

Response #14

Unfortunately, a post-earthquake DEM for this area is not available. Also, we wish to point out that the earthquake did produce significant differences in elevation, but these are localized close to the fault rupture.

Comment #15

6/7: Why did you use two pre-earthquake scenes if the aim was to map post-earthquake changes? And one of these was a Landsat image with very coarser resolution than the others (See table 1)

Response #15

The use of multiple scenes is desirable in studies that requires to define a pre-earthquake background level of (rainfall-induced) landsliding (e.g., landslide rates, landslide patterns, etc.) so that the earthquake-dependent contribution can be extracted. Using a single scene would be questionable because a normalization, e.g. by using storm rainfall, cumulated rainfall, etc., cannot be verified.

Regarding Landsat's low resolution, we are aware of that, but we still deemed preferable to include this map rather than providing only one pre-earthquake image. The readers / users of the dataset can make their own evaluations on whether to use this map or discard it.

Comment #16

6/9-10: Why did you delineate the co-seismic landslides? This has been done by at least 4 other researchers?

Response #16

We needed to delineate them by ourselves to be able to provide a fully consistent multitemporal dataset. Differently, we would be unsure whether coseismic and postseismic maps are complete/reliable to the same extent. With this regard, we saw that different mappers can obtain different results in a small area, such as the control area we used in our study (see Figure 7 in the manuscript). Additionally, in the new section we added in the *manuscript named "3.1.4 Comparison with existing inventories", we could check the differences between the inventories performed by Dai et al. (2011), Xu et al. (2014) and Tang et al. (2016). We conclude that the differences are important and, therefore, it reinforces the idea of performing a new mapping although previous ones already existed.*

Comment #17

6/12 and Figure 4: How good can you separate debris flows from channel deposits? Debris flows end up in the river channels in such a steep environment.

Response #17

It is true that at the debris flow depositional area, the difference between debris flows and channel deposits can be quite challenging as both deposits are mixed. In case that the remobilization of the channel deposits occurs before than the debris flow deposition, the latter will be easily mapped. Conversely, the debris flow fan will be underestimated. However, in our study area, the debris flow deposits are deposited in a relatively flat deposition area avoiding the spreading of the deposit (Figure 4 in the manuscript). Therefore, the underestimation of the depositional area compared with the runout is quite small and it does not have a high influence for area assessment purposes.

Comment #18

Table 1: Country should be county

Response #18

Corrected here and elsewhere in the text.

Comment #19

Figure 3: A comparison with Tang et al. (2016) who did the same would be relevant in the analysis section.

Response #19

A comparison with Tang et al. (2016) has been carried out. For the ease of visualization, a figure comparing the two different mapping methods has been added.

Comment #20

Figure 4 and 5: these are also very similar to the ones in Tang et al. (2016)

Response #20

These figures are necessary to clarify to the readers the classification of landslides that we used (which is different from that of Tang et al.) and to exemplify what each level of activity means (this is not present in Tang et al., who only show two "examples of changes in landslide activity" without referring to the levels of activity explicitly). Furthermore, we mapped different types of landslides which were not considered in Tang et al. (2016) such as "channel deposits" and the differentiation between "hillslopes" and "channelized debris flows".

Comment #21

12: Uncertainties. Did you only map one small watershed by all mappers? This test area seems to be rather straightforward? It would have been good to show more on the background of the mappers, in terms of experience and background knowledge, and how the results were for all mappers individually.

Response #21

Yes, only this watershed was mapped by all mappers for testing purposes, because it contains all types of instabilities and activity levels present in the study area. Therefore, the results of these two features can be compared between all mappers (results for each mapper can be found in the supplementary material of Fan et al. (2018a). We decided to use this control area as a mean to quickly get an estimate of the error that could be produced by manual mapping performed by different subjects. ***As far as we know, this has not been done at all in other***

multitemporal inventories performed through manual mapping. *We appreciate the suggestions of the referee, though, as it would be interesting to be able to quantify the role of different background and experience of the mappers, even though they agree on the same sets of rules for landslide identification and classification. However, a much larger area mapped by all mappers would be necessary for this, which is very time consuming, and this goes beyond the scope of this paper.*

Comment #22

Also, comparison with other inventories generated by others would have been relevant.

Response #22

Please refer to our Response #5.

Comment #23

Table 3: consider rounding off the values.

Response #23

We believe the values should reflect the actual sizes and volumes. In this way, they are verifiable from the shape files that are provided in the repository.

Comment #24

Figure 7: provide more description and conclusion on the results of the area-frequency analysis.

Response #24

More description has been added to the "Descriptive statistics" part. More detailed information about the area-frequency analysis can be found in Fan et al. (2018).

Comment #25

15/18 : Describe more how the multiple dates of occurrence for so many watersheds were collected. How many surveyors? How often did they visit the areas? Etc.

Response #25

Most of the debris flow were obtained from literature review which includes 76 references (see file named "References of data sources" in the repository). For the bigger and most catastrophic events, we performed field investigations and interviews to the local residents with a minimum of two surveyors. There not exists a fixed period where we go to the field as it mostly depends on the rainfall, which is the most important triggering mechanisms for the post-seismic events. We also collected information form the monitoring system that SKLGP has installed in some catchments (see Figure 1). We clarified this in the text.

Comment #26

16/1-2: for how many of the debris flow watersheds was it possible to get rainfall data within 5 km?

Response #26

391 over 527.

Comment #27

16/12-14: describe the method in more detail and give reference to other work.

Response #27

We added information to describe the method and references to other works.

Comment #28

Table 4: how was the volume of the deposits determined?

Response #28

These events have been taken from the literature. Therefore, it will depend on each author.

Comment #29

Figure 8: Is this not already published?

Response #29

It is not published as we made this figure specifically for this publication.

Referee #3 – T.W.J. van Asch

Comment #1

This paper gives a detailed and useful introduction to two very interesting multitemporal data sets which are probably the first data sets free available for the scientific community. The first data set is a multi-temporal polygon-based inventory of pre and co-seismic landslides, post-seismic remobilizations of co-seismic landslide debris, and post-seismic landslides induced by the Wenchuan earthquake (2008) in Sichuan province China. The second dataset contains information of the debris flows that occurred from 2008 to 2017 in the same area together with information on their triggering rainfalls recorded by a network of rain gauges. The two multi temporal data sets, which are made freely available, offer a good opportunity to analyze, at various scales, the patterns of enhanced land sliding caused by the earthquake. The first data set gives insight about the types and distribution of co-seismic landslides and their types of reactivation. It opens the way for scientist to analyze the factors influencing the distribution of co-seismic landslides, to make comparisons with the distribution of co-seismic landslides in other earthquake area, to analyze the factors causing the reactivation of these landslides and to explain the decrease in temporal frequency. And last but not least the data offers insight in the temporal evolution of the source materials for debris flows which is important for the modelling and understanding of the decrease debris flow frequency after the earthquake. The second data set about the temporal evolution of debris flows in the Wenchuan seismic area is a very rich source of information due to the large number of debris flows which are registered. The combination with information about the triggering rainfall data make it possible to construct general ranges in rainfall thresholds and more specific thresholds in relation to available source material and catchment characteristics. The detailed information about the catchment morphometry in the form of DEMS, time of occurrence of debris flows, antecedent rainfall patterns, available source materials and last but not least runout volumes at the outlet of the catchments make it possible to tests and bench marking all kinds of very detailed to more general debris flow models following different concepts with a very detailed to a more general character.

Response #1

Dear prof. van Asch,

We thank you for taking the time to review our manuscript. It is really a honour to learn that you deem our work very valuable. We sincerely appreciate your positive comment. Please find our point-by-point reply below.

Comment #2

The paper is a good guide for the data sets but some parts need a bit more explanation. I do not understand how the distribution of co-seismic landslides can give insight in the mechanism of an earthquake.

Response #2

For instance, a study made by Keefer (1984) and Rodríguez et al. (1999) found a correlation between the magnitude of the earthquake and the distance of landslides to the co-seismic fault. It has been also clarified in the text

Comment #3

We need also more comments on the different ways the co-seismic landslides are mapped in the past, the variety in interpretation of individual landslides and their presentation in maps (as points or polygons) and the consequences for analysing these kind of data sets.

Response #3

In the past, five inventories have been performed in the Wenchuan earthquake-affected area by Gorum et al. (2011), Dai et al. (2011), Xu et al. (2014), Li et al. (2014) and Tang et al. (2016). They were mapped either as points of the landslide scar areas or polygons with a different degree of accuracy (see Tang et al., 2016) and without distinction between the different types (landslides, debris flows, etc). Both accuracy and representation (as points or polygons) have direct implications for the analysis of the area-frequency distribution and the consequent hazard and risk assessment as well as the analysis of the controlling factors. Additionally, the distinction between different types of landslides accounts for individual analysis according to its nature. It has been also clarified in the manuscript

Comment #4

I would like to ask the authors why they think their mapping methodology has delivered the most reliable data set. The mapping of the landslides has been carried out by 5 interpreters following a set of common rules (see Fig 6). The authors mention also a methodology given by Harp et al 2006. We need more information about the criteria used by the mapping of these landslides.

Response #4

This is the most complete inventory of co-seismic and post-seismic landslides performed and freely available of the Wenchuan earthquake-affected area so far. Our method has a key point compared with earlier works carried out at the same area (Tang et al.; Yang et al.; Zhang et al.). We actually re-mapped and thus quantified the remobilised areas on each imagery rather than providing a qualitative estimation of the activity level. We quantified changes of the level of activity based on the actual polygon-mapping of the remobilised areas (and not on qualitative activity levels), we discriminated between different types of landslides and their location and we investigated a much larger and more representative area. We have now highlighted this in the revised manuscript.

Comment #5

In the temporal data set of co-seismic landslide and post seismic reactivation and new landslides are also included debris flows which are small debris flows (hillslope debris flows and so called channel deposits). The question arises what is the difference between these debris flows and the debris flows incorporated in the second data. Probably the two types of debris flows in the first data set have a limited displacement (not reaching the outlet of the catchment. The firs type are so called hill slope debris flows while the second type are channelized debris flows with a limited displacement. A significant amount of materials are involved in these channel deposits , which of course are very important source areas for future debris flows because the highest concentrations run-off water during future events are found in these channels. I suggest to call these two types :a)hills slope debris flows with limited run -out b) mainly channelized debris flows with a limited run-out.

Response #5

Actually, in Dataset1 we have two type of debris flows: hillslope debris flows, which are found along the hillslopes, and channelized debris flows, which are found into small channels. Then, the channelized deposits are large amounts of accumulated debris, found in the main channels, were clear remobilizations could not be identified. Furthermore, the source area of these materials is not known as they come from different debris flows and slides (debris and rock slides, debris and rock falls) that occurred upstream. Conversely, the debris flows reported in Dataset2 are big events that reached or approached the outlet of the catchment affecting *facilities and/or the population. In such case, the material can come from slides, hillslope and channelized debris flow and, mainly, form the existing the channel deposits material, all of them presented in Dataset1. This has been clarified in the text.*

Comment #6

Can you also describe their relation with the co- seismic landslides. Give also information in the text about the time period in which these landslide reactivation in the form of debris flows occurred: just after the earthquake or over a longer period?

Response #6

A great number of reactivations in the form of debris flows were identified within the first three years after the earthquake (2008-2011). Then, during the following years (2013 and 2015), the number of debris flows decreased considerably although a high amount of co-seismic material is still present in the hillslopes (Fan et al., 2018a). It suggests that the effects of the earthquake will be shorter than what it was initially expected (Huang and Fan, 2013). Some ongoing studies suggest that the changing in the properties of the co-seismic deposits, such as grain coarsening, my play a key role. It has been clarified in the text.

Comment #7

In Figure 4 you add a third type of debris flow namely "debris flows in a channel". What is the difference with the channel deposits? So I would ask for a more precise description of these types of debris flows?

Response #7

The difference between debris flow in a channel and channel deposits can be found in Fan et al. (2018a) and has been explained bellow. It has been also clarified in the text.

Debris flows were mapped when a fine-material texture along a preferential path could be identified. They can be found along the hillslopes (hillslope debris flows) or into channels (channelised debris flows). Large amounts of accumulated sediments are generally found in the main channels, but in many cases clear remobilisations could not be identified, hence such deposits were mapped as channel deposits.

Comment #8

The level of activity in A1, A2 and A3 are defined as a percentage of area which is remobilized Are these activated areas delineated and do we get an impression of the degree of displacement (limited displacement or larger displacement in the form of debris flows see above). I cannot see that in Fig 3 and I have no possibility to open the shape files to look in detail.

Response #8

Yes, the remobilised area has been delineated. In the inventory it can be compared the position of the co-seismic deposits and the one of the post-seismic remobilizations. So, the displacement can be calculated.

Comment #9

Regarding the debris flows: can the authors also give an estimate about time period in which the pre-earthquake registered debris flows were formed?

Response #9

Unfortunately, we do not have a record of the previous debris flows occurred in the area. The most estimate period can be obtained from the year in which they were mapped (2005 and 2007).

Comment #10

In the debris flow data base we have no information whether the debris flows started as sliding mass failures or by run-off erosion, which is very important for the type of modelling and for understanding the type of meteorological thresholds.

Response #10

We agree with the referee that the initiation mechanisms is important for modelling purposes and definition of rainfall thresholds. According to our experience in the study area, these two processes often concur to the same event, and their relative importance evolves with time during an event. For some debris flows, the event may start as a sliding mass failure from the coseismic landslide deposits, and when the rain is intense, it can generate concentrated surface run-off causing run-off erosion. For some other events, depending on the type of material and terrain, run-off erosion may occur first, and the subsequent entrainment may cause incision and failure of deposits and also erosion and incision of the channel.

The processes vary case by case. However, this information is not available in all the papers and in some cases is just estimated or guessed. Therefore, we considered that it should be carefully checked, case by case, by the users of our dataset, when necessary, using the references that we provide therein.

Comment #11

I do not understand in the caption of Table 4 the difference between “Time 24” and “T”.

Response #11

Actually it is “T_Comment” instead of “T”. “Time_24_” is a numeric field with the time of occurrence of the debris flow. T_Comment is a text field where it is clarified if “Time_24_” corresponds to the initiation or deposition of a given event. In few cases “Time_24_” also reports a range of days where the debris flow occurred. It has been clarified in the manuscript.

Comment #12

The available material during the initiation of the flow changes with time. From where did you get this information? From the first data set about the Multi-temporal inventory of landslides?

Response #12

We got this information form other publications that are reported in the database (see “Reference of Data source” in the DF_RG_inventory.xlsx file).

Comment #13

The authors also mention a general travel time of 1 hr which makes it possible to get an estimate for the initiation time of the debris flow (important value for calibrating and validating models). I wonder whether that is not a too general statement. Are there no large variations in travel time of debris flows between catchments?

Response #13

The referee is right as in our study area there are catchments of different sizes, which influences the travel time. Additionally, the position of the co-seismic deposit where the debris flow initiate and the presence of deposits blocking the river and mitigation works, among others, could also increase the travel time. We delete this sentence to avoid any misunderstanding.

Comment #14

To come to a conclusion I would say that these data sets merit to be published and I advise minor revision to give some more explanations on certain aspects.

Response #14

Thank you very much for your positive comments and suggestions. We really appreciate all of them

Referee #4 – T. Gorum

Comment #1

The Wenchuan earthquake is a major event where many slope failures have been recorded (200,000>) in one single event. I think this is the most important earthquake in the last century in terms of the amount of debris that exposed. The importance of this earthquake in landslide science is not only due to the number of landslides it triggered. The change in the type and size of the landslides after the earthquake showed that the effects of the earthquake could last much longer than expected which is emphasized in the manuscript. The dataset revealed by this study was produced from very high resolution images to map the pre- and coseismic landslides, post-seismic reactivations of coseismic landslide debris and new landslides in the main earthquake struck the region. Unlike other studies in this respect, this contribution is based on the extensive results of the earthquake and made the data freely available to other researchers which are quite important to improve the current knowledge state regarding the coseismic landslide hazard. Moreover, the two multi-temporal data sets presented in this study have the potential to contribute for better understanding the relaxation phase of the landscape after major earthquakes and the full impact of earthquake-induced landslides on the landscape. This will allow for a more comprehensive understanding of temporal perturbations caused by strong earthquakes. My suggestion is that these two valuable datasets worth to be published after minor revisions.

Response #1

Dear Prof. Gorum,

We thank you for reviewing our manuscript. We sincerely appreciate your positive review. Please find our detailed reply below.

Comment #2

Please clarify the main difference between debris flows in different data set of co-seismic landslide and post-seismic reactivation and new landslides. Some of them, especially post-seismic reactivations, looks like torrents and/or channelized debris flows.

Response #2

Debris flows exhibited a finer material texture along a preferential movement path. They were found along the hillslopes (named hillslope debris flows) and into small channels (named hillslope debris flows). *.It has been clarified in the text*

Comment #3

Please consider changing the title of 3.1.3 “Simple statistics” to “Descriptive statistics”.

Response #3

Done for 3.1.3 and also for 3.2.3.

Comment #4

In general, the manuscript is lack of a rigorous description of the landslide volume calculations. Please give more details about the volume estimation of the debris flow deposited at the fan area and also for other volume estimation that has been used in the study for landslides.

Response #4

The volume of the debris flow deposited at the fan area (Dataset2) has been obtained from the existing literature. Regarding the volume calculated for the other landslides, it is true that just little information has been given about this. Actually, it has been done on purpose as the objective of the paper is to give a general vision of the prepared inventory and a few examples of different analyses that can be performed with this. Nevertheless, more information about the area-volume relationship can be found in Fan et al. (2018a). It has also been included bellow:

The volume (V) of the co-seismic landslides was estimated from the mapped areas using the empirical relation suggested by Xu et al. (2016), which was calibrated on a large set of co-seismic landslides triggered by the Wenchuan earthquake:

$$V = 1.315 \cdot A^{1.208}$$

where A is the landslide area (m2) and V is the estimated volume of the landslide (m3). The relation brings an uncertainty (±1 standard deviation in the calibration set) on the calculated volume of +14.7%/-13.8% (Xu et al. 2016). We employed the same volume-area relationship to calculate also the volumes of post-seismic remobilisations and new landslides, as we did not have any means to constrain them further. However, this assumption might cause an overestimation of the post-seismic landslide volumes, as bedrock landslides (a portion of the co-seismic landslides) are generally deeper than soil/debris landslides (the post-seismic remobilisations of the co-seismic deposits) with the same area, as noted by Larsen et al. (2010) and Parker et al. (2011).

The document "Readme.doc", attached in the repository, has been pasted here for the ease of referee 2. This document explains the different files found in the repository.:

Dataset 1

It contains shapefiles of the pre-, co-, and post-seismic landslides and the catchments where they are located. The area of study has an extension of 462.5 km^2 and it is located in the 2008 Wenchuan Earthquake epicentre. The information is distributed in 7 shapefiles. Information about each layer and attributes is detailed in Tab. 1.

Table 1 Reference image used to map the landslides, acquisition date, attributes and description of each layer contained in the dataset.

Name of the layer (.shp)	Reference image: source / resolution / band	Acquisition date	Attributes
DF_Catchments		-	Shape, Name, CID, Country, Area, Grad_chan, Grad_Mchan, Grad_catch, Leng_chan, Drain_Dens, Reli_Mchan, Reli_chan, Reli_catch
2005	Spot 5 / 2.5 m / multispectral	Pre-earthquake (July 2005)	ID, Shape, Area, CID
2007	Landsat 4 / 30 m / multispectral	Pre-earthquake (September 2007)	ID, Shape, Area, CID
2008	Aerial photos / 1-2.5 m / RGB-panchromatic	Co-seismic (May-July 2008)	ID, Shape, Area, Type, CID
2011	Aerial photos + Worldview 2 / 0.5-1 m / RGB-pansharpened	Post-seismic (April 2011)	ID, Shape, Area, Type, Act_level, CID
2013	Aerial photos + Pleiades / 0.5-2 m / RGB-panchromatic + multispectral	Post-seismic (April 2013)	ID, Shape, Area, Type, Act_level, CID
2015	Spot 6 / 1.5 m / pansharpened	Post-seismic (April 2015)	ID, Shape, Area, Type, Act_level, CID
2017	Spot 6 / 3 m / RGB	Post-seismic (April 2017)	ID, Shape, Area, Type, Act_level, CID

2018	Spot 6 / 3 m / RGB	Post-seismic (April 2018)	ID, Shape, Area, Type, Act_level, CID
Attributes: Shape (type of element: polygon, line, point); Name (Name of each catchment); CID (identifier for each catchment); County (Name of the county where the catchment is located); Area (Area of each element in m^2); Grad_chan (mean slope of the whole channels present in the catchment in decimal degrees); Grad_Mchan (mean slope of the main channel present in the catchment in decimal degrees); Grad_catch (mean slope of the catchment in decimal degrees); Leng_chan (total length of the channels present in the catchment in m); Drain_Dens (Leng_chan/Area in m^{-1}); Reli_Mchan (Relieve of the main channel: highest altitude minus lowest altitude of the main channel in m), Reli_chan (Relieve of all the channels present in the catchment: highest altitude minus lowest altitude of the channels m), Reli_catch (Relieve of the catchment: highest altitude minus lowest altitude of the catchment m); ID (identifier of each element); Type (type of landslide: s – slide; d – debris flow; cd – channel deposit); Act_level (level of activity of the landslide: 0 – activity level A0, dormant landslide; 1 – activity level A1; 2 – activity level A2; 3 – activity level A3; 4 – new landslide).			

Dataset 2

It contains the records of the debris flows that occurred from 2008 to 2017 in Wenchuan (W), Pengzhou (P), Mianzhu (M) and Anxian (A) countries and the information on their triggering rainfalls recorded by a network of rain gauges. Information about each layer and attributes is detailed in Tab. 2.

Table 2. Structure of the dataset of debris flows and their triggering rainfalls.

Folder name	File name	File type	Layers/sheets	Attributes (columns)
DF_RG_inventory	DF_RG_inventory	Shape file (.shp) and spreadsheet (.xls)	debris_flows	DF_ID, CID, Gully_name, Latitude, Longitude, Year, Month, Day, Time_24h_, T_Comment, Source_vol, Depo_vol, List_of_RG, Monitoring, Reference
			rain_gauges	RG_ID, CID, coordinates, temporal resolution, units, data references
R_DF_ID_X*	A_B_CDEF	Spreadsheet (.xls)	-	date and time, amount of rain
Attributes: DF_ID: identifier of the debris flow; CID: identifier of the catchment to which the debris flow or the rain gauge belong; Gully_name: name of the catchment; Latitude: latitude of the debris flow event (º); Longitude: longitude of the debris flow event (º); Year: year the debris flow event occurred; Month: month the debris flow event occurred; Day: day the debris flow event occurred; Time_24h_: time at which the debris flow occurred (24 h); T_Comment: specifications on the time of occurrence of the debris flow (initiation, deposition or range of days); Source_vol: available material during the initiation of the debris flow (m^3); Depo_vol: volume of debris flow deposited at the fan area (m^3); List_of_RG: list of rain gauges (identifier) located in proximity to the debris flow event that were actively recording throughout the time window of interest for that debris flow;				

Monitoring: specifies if additional monitoring data are available for that event (Y: yes; N: no); References: source of each debris flow event. * one folder for each debris flow event being "X" the debris flow event identifier (DF_ID). Each folder contains the rain gauges located within a distance of 5 km for a given event. "A" indicates the relative position of each rain gauge from the debris flow event in ascending order; "B" refers to the rain gauge identifier (RG_ID); C, D and E indicate the year, month and day of the debris flow event, respectively, and F refers to the starting time of the rain. Rain is expressed in mm. Each spreadsheet provides data from 7 days before to one day after the date associated with the debris flow event (DF_ID). Full data series are available, from the authors upon request, for further analysis.

Examples of well-monitored catchments

It contains two excel files with detailed information about Wenjia Gully, at Miangzhu Country, and Hongchun and Er gullies both located at Wenchuan country. Information about each layer and attributes is detailed in Tab. 3.

Table 3. Structure of the dataset for the monitored catchments.

File name	File type	Sheets	Attributes (columns)
Er_vel_rain_disc_dens	Spreadsheet (.xls)	debris_flows	Latitude and Longitude of each station (º),Rainfall intensity measured at R1 (mm/h); Discharge measured at S1, S2 and S3 (m^3/s); Flow density measured at S1 (g/cm^3) and Flow depth (m) vs flow velocity (m/s) measured at S1 (Peng et al., 2018)
Rainfall data	Spreadsheet (.xls)	Qingping_a	Rain gauge coordinates, Date, Daily rainfall (mm), Cumulative rainfall (mm) (You et al., 2018)
		Qingping_b	Rain gauge coordinates, Date, Time (h), Hourly rainfall (mm), Cumulative rainfall (mm) (You et al., 2018).
		Hongchun	Rain gauge coordinates, Date, Time (h), Hourly rainfall (mm), Cumulative rainfall (mm) (Tang et al., 2011)
		Er	Rain gauge coordinates, Date, Time (h), Hourly rainfall (mm), Cumulative rainfall (mm) (Cui et al., 2018)

Doc files:

"References of data sources.docx": It contains a list of all the references.

Short Comment #1 – W. Yang

Comment #1

The 2008 Wenchuan earthquake triggered more than 190,000 landslides over 100,000 km^2 (Xu et al., 2013). This amount of coseismic landslides significantly altered local strata leading to enhanced post-seismic landsliding which may last for many years. Therefore, studying post-seismic landslide evolution is crucially important for the mountain hazard research groups as well as disaster management communities. Fan et al. provide a multi-year landslide inventory in the epicentre area and some debris flow data as well as precipitation data in the Wenchuan earthquake affected region. These landslide data in such a vast region is very scares. The multi-year landslide inventory in the Wenchuan region is very difficult to acquire, because the region is very large and also remote sensing images of this region are frequently contaminated by heavy clouds. From their work, it is obvious that Dr. Fan and her colleague devoted massive amount of money, time and energy in collecting and interpreting these data. If these datasets can be openly published, it has the potential to greatly push forward the frontiers of the post-seismic landsliding studies.

Response #1

Dear Dr. Yang, we are very grateful for your positive comment. We too believe that the availability of input datasets is of fundamental importance for a variety of studies and analyses through which the research community can improve the understanding of post-seismic landscape processes substantially. This is the spirit with which we compiled our datasets, that we are now making them available to the community.

Two multi-temporal datasets to track the enhanced landsliding after the 2008 Wenchuan earthquake

Xuanmei Fan[1], Gianvito Scaringi[2], Guillem Domènech[1], Fan Yang[1], Xiaojun Guo[3], Lanxin Dai[1], Chaoyang He[1], Qiang Xu[1], Runqiu Huang[1]

[1]State Key Laboratory of Geohazard Prevention and Geoenvironment Protection, Chengdu University of Technology, Chengdu, 610059, China
[2]Institute of Hydrogeology, Engineering Geology and Applied Geophysics, Faculty of Science, Charles University, Prague, 128 43, Czech Republic
[3]Key Laboratory of Mountain Hazards and Surface Process, Institute of Mountain Hazards and Environment, Chinese Academy of Sciences, Chengdu, 610041, China

Correspondence to: Xuanmei Fan (fxm_cdut@qq.com), Xiaojun Guo (aaronguo@imde.ac.cn) and Qiang Xu (xq-68@qq.com)

Abstract. We release two datasets that track the enhanced landsliding induced by the 2008 M_w 7.9 Wenchuan earthquake over a portion of the Longmen mountains, at the eastern margin of the Tibetan plateau (Sichuan, China). The first dataset is a geo-referenced multi-temporal polygon-based inventory of pre- and coseismic landslides, post-seismic remobilisations of coseismic landslide debris, and post-seismic landslides (new failures). It covers 471 km^2 in the earthquake's epicentral area, from 2005 to 2018. The second dataset records the debris flows that occurred from 2008 to 2017 in a larger area (~17,000 km^2), together with information on their triggering rainfall as recorded by a network of rain gauges. For some well-monitored events, we provide more detailed data on rainfall, discharge, flow depth and density. The datasets can be used to analyse, at various scales, the patterns of landsliding caused by the earthquake. They can be compared to inventories relative to past or new earthquakes or other triggers to reveal common or distinctive controlling factors. To our knowledge, no other inventories that track the temporal evolution of earthquake-induced mass wasting have been made freely available thus far. Our datasets can be accessed from https://doi.org/10.5281/zenodo.1405489. We also encourage other researchers to share their datasets to facilitate research on post-seismic geological hazards.

1 Introduction

1.1 Earthquake-induced enhanced landsliding

Large earthquakes cause major disturbances to the patterns of erosion and sediment export from mountain belts (e.g., Keefer, 1994; Dadson et al., 2004; Hovius et al., 2011; Parker et al., 2011; Huang and Fan, 2013; Li et al., 2017). Thousands of landslides can be triggered by the seismic shaking. These coseismic landslides generate large amounts of debris, part of which will reach large streams and form landslide-dammed lakes that impound large volumes of water and sediments (Fan et al., 2012, 2017b; Tang et al., 2018). More debris will deposit, with marginal stability, high on the slopes and in low-order channels (Meunier et al., 2008; Gorum et al., 2011; Kargel et al., 2016; Fan et al., 2018a, 2018b). It will be remobilised easily by minor storms (Dadson et al., 2004; Lin et al., 2006; Huang and Fan, 2013; Fan et al., 2018b) and generate large flow-like landslides (Xu et al., 2012; Hu et al. 2017, 2018a, 2018b, 2018c). The earthquake-induced enhanced weakening and weathering of rock and soil masses also will cause delayed slope failures and sustain high erosion rates for a long time (Koi et al., 2008; Parker et al., 2015; Fan et al., 2017a, 2018d; Scaringi et al., 2018). These processes are a major source of hazard to the population and the infrastructure. Earthquake-triggered chains of geohazards are major contributors to the tolls of damage and fatalities and to the costs of reconstruction and recovery of the socioeconomic fabric after large earthquakes (Huang and Fan, 2013; Wang et al., 2014).

Observations on the evolution of mass wasting after recent major earthquakes reveal a peak of landslide rates (remobilisations of coseismic landslide deposits and post-seismic landslides) soon after the earthquakes, followed by decay and normalisation within less than a decade (Fan et al., 2018a; Hovius et al., 2011; Marc et al., 2015; Zhang et al., 2016; Zhang and Zhang, 2017). The reasons for this normalisation, which seems quicker than that of the sediment export by non-landslide processes (Ding et al., 2014; Wang et al., 2015, 2017), are still poorly understood. Various processes, such as the progressive depletion of the debris, grain coarsening and densification, restoration of the vegetation cover and bedrock healing have been shown to play a role (e.g., Shieh et al., 2009; Zhang et al., 2014; Hu et al., 2018c; Yang et al., 2018). Analyses of complete inventories that track the decay of landslide rates, together with laboratory and field-scale investigations and physically-based models, can certainly provide further insights.

1.2 Multi-temporal inventorying of landslides

Landslide mapping and inventorying at various scales are fundamental tools to investigate the spatial and temporal patterns of mass movements quantitatively, obtain insight on their failure-runout mechanisms and damage, and reveal topographic, seismic, geological, hydrological, climatic, biological and anthropogenic preconditions and causal factors to their distribution and fate (e.g., Guzzetti et al., 2002, 2009, 2012; Corominas et al., 2008; Galli et al., 2008; Harp et al., 2011; Parker et al., 2015; Gariano and Guzzetti, 2016; Broeckx et al., 2018). Coseismic landslide inventories are compiled after major events with increasing quality and completeness (Keefer, 2002; Schmitt et al., 2017; Tanyas et al., 2017). They are fundamental for assessing the extent of the earthquake-affected areas and drive the post-earthquake emergency response, as they are the basis for susceptibility, hazard and risk analysis. Additionally, they can help reconstruct earthquake mechanisms (Gorum et al., 2011; Fan et al., 2018c): for instance, studies by Keefer (1984) and Rodriguez et al. (1999) first related the earthquake magnitude and the spread of landslides from the seismogenic fault. Besides, complete and detailed inventories are necessary to evaluate the landscape response to earthquakes quantitatively, and to calibrate descriptive and predictive models effectively (Xu et al., 2014; Marc and Hovius, 2015; Marc et al., 2016a, 2016b, 2017). Many coseismic landslide inventories have been released, and some of them were collected in a freely accessible repository by Schmitt et al. (2017). We believe that this can promote standardisation of data collection and presentation and facilitate meta-analyses and modelling efforts greatly. Several inventories were compiled for the Wenchuan earthquake-affected area (Gorum et al., 2011; Dai et al., 2011; Xu et al., 2014; Li et al., 2014; Tang et al., 2016). Landslides were mapped either as points (identifying the landslide scar) or polygons, with different degrees of accuracy (see Tang et al., 2016), and with or without distinction between landslide types (slides, flows, etc). Both accuracy and representation (as points or polygons) have direct implications for the analysis of landslide size-frequency distributions and hazard and risk assessments, as well as for the analysis of controlling factors. Additionally, the distinction between different types of landslides allows for dedicated analyses of distinctive controlling factors and characteristics.

Landslide inventories that include several temporal scenes before and after major earthquakes are much less common. In fact, the interest around the temporal evolution of landsliding after major earthquakes has increased greatly in the past decades, particularly after the 1999 M_w 7.7 Chi-Chi and 2008 M_w 7.9 Wenchuan earthquakes (Dadson et al., 2004; Fan et al., 2018a, 2018b; Hovius et al., 2011; Marc et al., 2015; Tang et al., 2016; Yang et al., 2016, 2018; Zhang et al., 2016; Zhang and Zhang, 2017) and has the potential to answer various research questions concerning, for instance, erosional patterns and morphological signatures in seismically active mountain ranges. Research has been facilitated by the increased availability of repeated and high-resolution remote sensing images (Fan et al., 2018b), and by near real-time monitoring networks (Huang et al., 2015). However, to our knowledge, none of the multi-temporal inventories of post-seismic landslides compiled so far have been released to open repositories. With this paper and the related datasets, we wish to share our mapping work and monitoring data to facilitate further analyses and meta-analyses by the research community. We also wish to encourage other researchers to share their data, with the aim of building a collection of datasets that will help advance the knowledge in the field.

2 Study area

Our datasets cover portions of the region affected by the M_w 7.9 Wenchuan earthquake at various levels of detail (Figure 1). The earthquake hit the Longmen mountains (Longmenshan) in west Sichuan, China, at the eastern margin of the Tibetan plateau on May 12th, 2008, with a fault rupture that propagated from the epicentre along the range for about 240 km (Gorum et al., 2011; Huang and Fan, 2013; Fan et al, 2018b). Details on the tectonic setting of the Longmenshan and on the Wenchuan earthquake mechanisms, as well as geological and geomorphological characterisations of the region, can be found in several earlier works (Qi et al., 2010; Dai et al., 2011; Gorum et al., 2011) to which the reader is referred for further information.

According to a recent inventory (Xu et al., 2014), the Wenchuan earthquake triggered almost 200,000 coseismic landslides over an area larger than 110,000 km^2. The total landslide area was estimated in about 1,160 km^2 (Xu et al., 2014), and the total landslide volume in the order of several km^3 (Parker et al., 2011; Li et al., 2014; Marc and Hovius, 2015; Xu et al., 2014, 2016). Rain-induced post-seismic failures of deposits of coseismic debris, often evolving into catastrophic debris flows and floods, have been occurring frequently since after the earthquake (Tang et al., 2009, 2011, 2012; Xu et al., 2012; Guo et al., 2016, 2017).

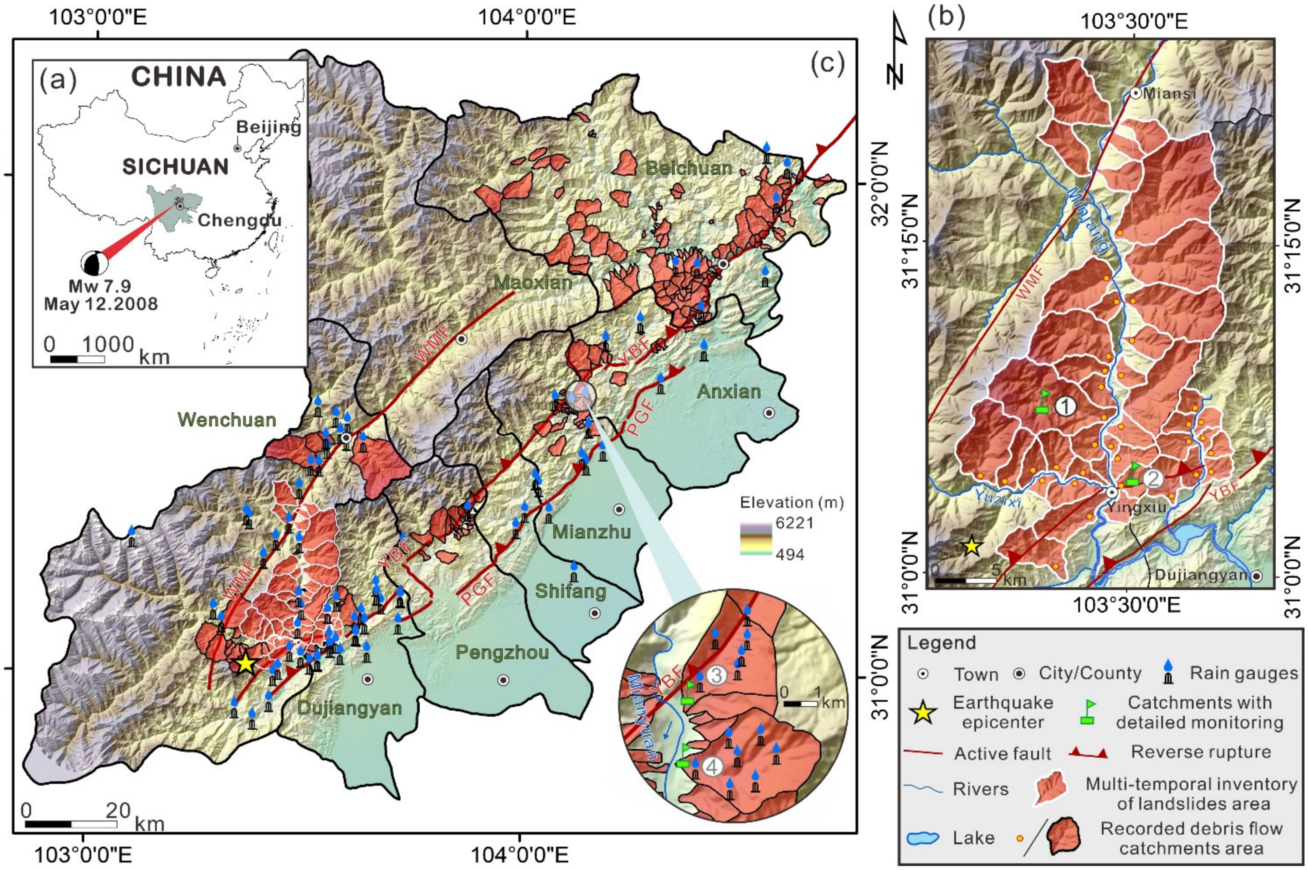

Figure 1. General view of the study area in Sichuan, China (a); Detail of the area in which the multi-temporal inventory of landslides was carried out (b); Detail of the area in which debris flows were recorded, with indication of their location and those of the rain gauges (c). Circled numbers (1-4) indicate well-monitored catchments.

2.1 Inventory of landslides

Our multi-temporal inventory of pre- and coseismic landslides, post-seismic remobilisations and new failures covers a significant portion of the earthquake's epicentral area. It is the largest area affected by the Wenchuan earthquake that has been covered by a detailed multi-temporal landslide inventory thus far (Fan et al., 2018a). The area comprises 42 catchments over 471 km^2 from the town of Yingxiu (the epicentre) to the town of Wenchuan (Figure 1b). It has been affected by coseismic landslides with a total volume in the range 0.8-1.5 billion m^3, as estimated through a set of first-order empirical area-volume scaling relationships (Parker et al., 2011; Xu et al., 2016). The reader is referred to Fan et al. (2018c) for a discussion on the reliability and uncertainties arising from the use of empirical area-volume relationships for the estimation of coseismic landslide volumes.

The region that we investigate has rugged mountains with elevations that climb rapidly from 420 m a.s.l. in the main river valley to the over 4,000 m a.s.l. of some mountain ridges. The slopes are generally steep, with more than half of them steeper than 36º. Two of the main faults of the Longmenshan, the Wenchuan-Maowen and the Yingxiu-Beichuan faults (e.g., Qi et al., 2010), delimit this study area. Beneath a dense vegetation and a variably-thick soil cover lie weathered and highly fractured rocks, mostly igneous (granite, diorite), though metamorphic and sedimentary rocks (schist, shale, sandstone, limestone) are also present, as well as recent Quaternary deposits. The climate is subtropical, affected by the monsoonal circulation, with 13 ºC of mean annual temperature and >1,250 mm/year of precipitation which mostly occurs in the summer months. The Min river (Minjiang), a tributary of the Yangtze river in its upper course, crosses the region through Wenchuan and Yingxiu and discharges, in average throughout the year, 452 m^3/s of water (Tang et al., 2011).

2.2 Inventory of debris flows and their triggering rainfalls

The dataset of debris flows and their triggering rainfalls covers 16,959 km^2, from the epicentre (near the town of Yingxiu) to the edge of the thrust-dominated portion of the seismogenic fault rupture (near the town of Beichuan). In this region, 527 debris flows affecting 244 catchments were identified. These catchments cover altogether about 1,581 km^2 (Figure 1c), and spread along 177 km out of the 246 km of the fault surface rupture.

The study area is mountainous with elevations from 420 m a.s.l. in the river valley up to almost 6,100 m a.s.l. on the ridges of the Hengduan mountains. A general northeast to southwest orientation is shown by the geological structures and the strike of the rock strata, and the bedrock outcrops are highly fractured and weathered. Most of the low-order channels are deeply cut and the slopes are steep, with a morphology that is strongly controlled by the high tectonic activity (Guo et al., 2016). The climate is generally monsoon-influenced, with precipitations concentrated in the summer months. However large variability exists within this larger region, with the central and southern parts receiving annual precipitations exceeding 1,200 mm and easily reaching 2,000 mm, and the western part being drier and receiving less than 800 mm/year of precipitation (Guo et al., 2016).

The complex geology and the patterns of precipitation (with frequent but localised rainstorms that can deliver hundreds of mm of rain in each event) make the area highly prone to the occurrence of debris flows. About 250 debris flows were recorded in the decades preceding the Wenchuan earthquake (Cui et al., 2008), and hundreds more were triggered after the earthquake, affecting more than 800 streams within the first two years (Cui et al., 2011). The characteristics of the rain events that triggered debris flows changed abruptly upon the earthquake, with triggering rainfall intensity and duration that dropped significantly, and subsequently exhibited a pattern of gradual recovery over a decadal time scale (e.g., Yu et al., 2014; Guo et al., 2016, 2017).

3 Data and methods

Here we provide details of the source data and the preparation of our inventories. We also include some figures and tables that illustrate the contents of the inventories and some simple analyses.

3.1 Multi-temporal inventory of landslides

3.1.1 Imagery, mapping technique, attributes

We compiled the inventory through visual interpretation (following Harp et al., 2011) of high-resolution aerial and satellite images (Spot 5, Spot 6, Worldview 2, Pleiades). In total, eight sets of images were acquired, covering the period from 2005 to 2018 (Table 1). We selected these scenes according to the availability, date of acquisition, coverage, absence of clouds and resolution. With respect to the targeted study region, the areal coverage of the images is close to 99% in 2007, 2011 and 2015, 97% in 2008, 95% in 2013, and 93% in 2005, 2017 and 2018. The 2011 scene was used as our geo-referencing base in ArcGIS environment (Environmental Systems Research Institute, Inc., United States) and the orthorectification was performed using the software Pix4D (Pix4D S.A., Switzerland). A 25-m resolution digital elevation model, obtained from the Sichuan Bureau of Surveying and Mapping, was used to delineate the catchment boundaries.

Our inventory (Figures 2-3) provides a polygon-based delineation of landslides that occurred before the earthquake (2005 and 2007 scenes), which can be used to define the pre-earthquake landslide rates and patterns in studies focusing on a short-term time window. The 2008 scene was used to delineate the coseismic landslides; the 2011, 2013, 2015, 2017 and 2018 scenes were used to identify the new landslides that occurred after the earthquake (i.e. the post-seismic landslides) and the remobilisations of coseismic landslides (i.e. the post-seismic remobilisations).

The landslide areas were differentiated into three types: slides, debris flows and channel deposits. Slides were mapped as such if preferential movement paths could not be identified in their debris-covered deposition areas. This type comprises debris and rock slides and debris and rock falls (see Hungr et al., 2014, for the definitions of the landslide types). This simplification derives from a lack of discernibility, in the remote sensing images, between these types of movement and their combinations. Differently, debris flows exhibited a finer material texture along a preferential movement path. They were found along the hillslopes (hillslope debris flows) and into small channels (channelised debris flows). Large amounts of accumulated debris were also found in main channels. The source area of these materials is not known as they come from multiple debris flows and slides located upstream, and in many cases clear remobilisations could not be identified. Therefore, these deposits were mapped as channel deposits. They are very important source areas for subsequent debris flows initiated by runoff erosion during intense storms. Some examples of landslide types are given in Figure 4.

It is worth noting that, differently from earlier works (Tang et al. 2016; Yang et al. 2016; Zhang et al. 2016), we quantified changes of the level of activity based on the actual polygon-mapping of the remobilised areas (Figure 5), we discriminated between different types of landslides and their location and we investigated a much larger and more representative area.

Nevertheless, for ease of visualisation and comparison of some results (see Figure 3 and Figure 6), we defined four levels of activity to classify the landslide remobilisations, following Tang et al. (2016). A level of activity A1 was assigned if less than 1/3 of the coseismic or post-seismic landslide area displayed signs of remobilisation; a level A2 was assigned if the remobilisation involved between 1/3 and 2/3 of the area; a level A3 was assigned if the remobilisation involved more than 2/3 of the area. Finally, a level A0 was assigned if no remobilisations were identified (i.e. the landslide was dormant or its movement was too slow to produce changes that could be seen from the available imagery).

Table 1. Reference images used to map the landslides, acquisition date and attributes of each layer contained in the dataset. An additional shape file is provided to define the catchment boundaries and have a simple characterisation (CID: catchment identifier, catchment name and county, gradient and internal relief, drainage density and channel length).

Name of the layer (.shp)	Reference image: source / resolution / band	Acquisition date	Attributes
DF_Catchments		-	Shape, Name, CID, County, Area, Grad_chan, Grad_Mchan, Grad_catch, Leng_chan, Drain_Dens, Reli_Mchan, Reli_chan, Reli_catch
2005	Spot 5 / 2.5 m / multispectral	Pre-earthquake (July 2005)	ID, Shape, Area, CID
2007	Landsat 4 / 30 m / multispectral	Pre-earthquake (September 2007)	ID, Shape, Area, CID
2008	Aerial photos / 1-2.5 m / RGB-panchromatic	Coseismic (May-July 2008)	ID, Shape, Area, Type, CID
2011	Aerial photos + Worldview 2 / 0.5-1 m / RGB-pansharpened	Post-seismic (April 2011)	ID, Shape, Area, Type, Act_level, CID
2013	Aerial photos + Pleiades / 0.5-2 m / RGB-panchromatic + multispectral	Post-seismic (April 2013)	ID, Shape, Area, Type, Act_level, CID
2015	Spot 6 / 1.5 m / pansharpened	Post-seismic (April 2015)	ID, Shape, Area, Type, Act_level, CID
2017	Spot 6 / 3 m / RGB	Post-seismic (April 2017)	ID, Shape, Area, Type, Act_level, CID
2018	Spot 6 / 3 m / RGB	Post-seismic (April 2018)	ID, Shape, Area, Type, Act_level, CID

Attributes: Shape (type of element: polygon, line, point); Name (Name of each catchment); CID (identifier for each catchment); County (Name of the administrative County where the catchment is located); Area (Area of each element in m^2); Grad_chan (mean slope of the whole channels present in the catchment in decimal degrees); Grad_Mchan (mean slope of the main channel present in the catchment in decimal degrees); Grad_catch (mean slope of the catchment in decimal degrees); Leng_chan (total length of the channels present in the catchment in m); Drain_Dens (Leng_chan/Area in m^{-1}); Reli_Mchan (Relieve of the main channel: highest altitude minus lowest altitude of the main channel in m), Reli_chan (Relieve of all the channels present in the catchment: highest altitude minus lowest altitude of the channels m), Reli_catch (Relieve of the catchment: highest altitude minus lowest altitude of the catchment m); ID (identifier of each element); Type (type of landslide: s – slide; d – debris flow; cd – channel deposit); Act_level (level of activity of the landslide: 0 – activity level A0, dormant landslide; 1 – activity level A1; 2 – activity level A2; 3 – activity level A3; 4 – new landslide).

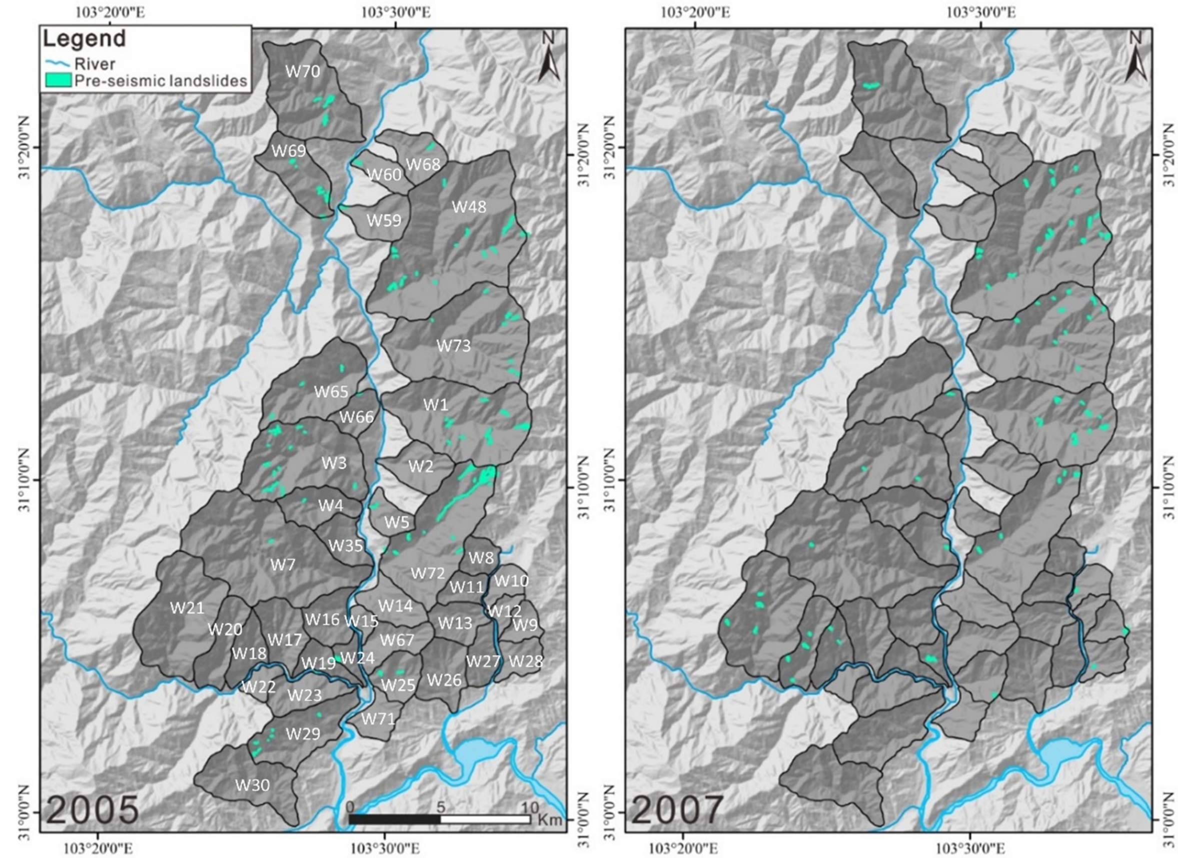

Figure 2. Landslides identified from remote sensing images recorded in 2005 and 2007 (pre-earthquake). The identifier for each catchment (see CID in Table 1) is shown in 2005.

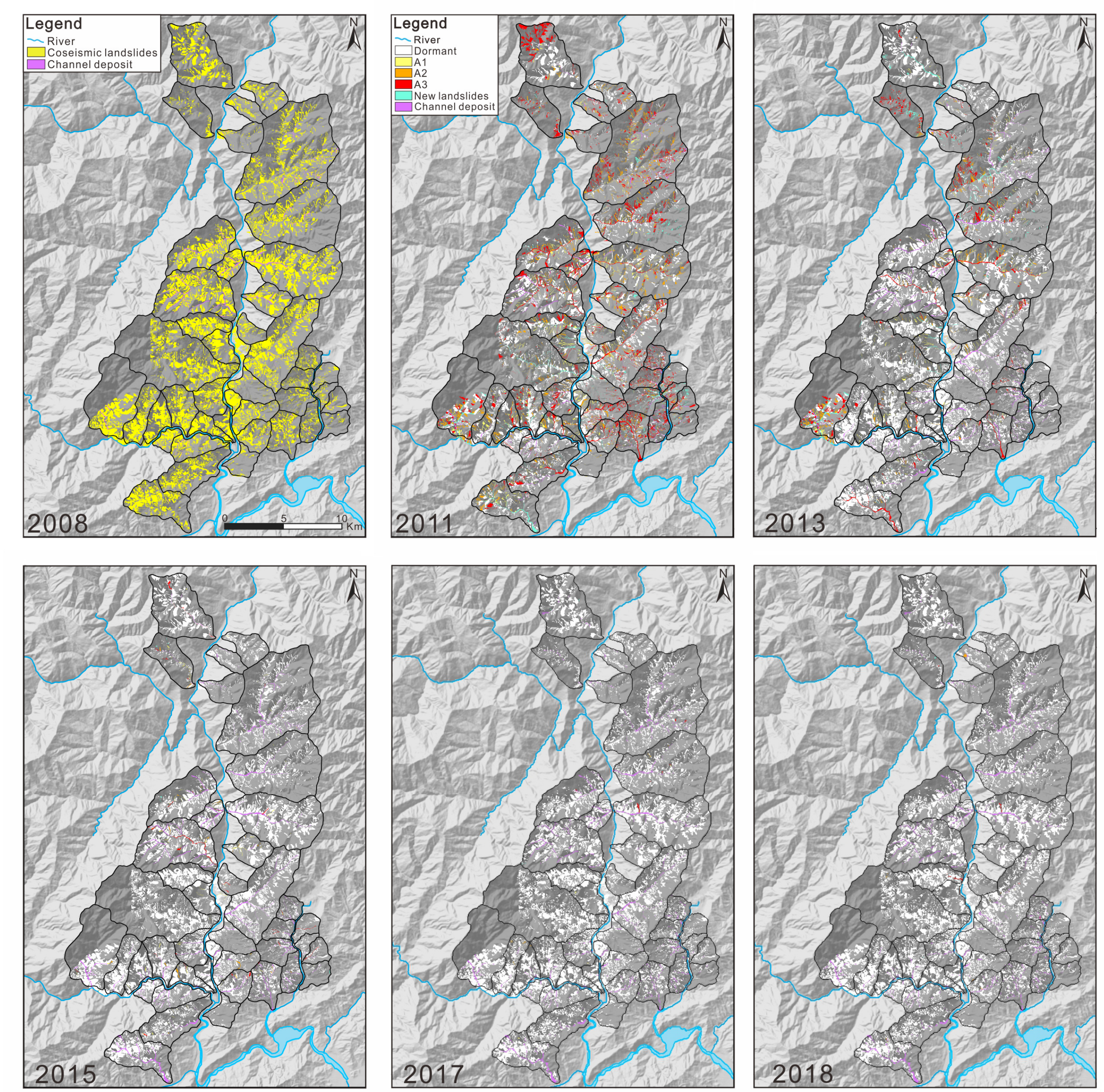

Figure 3. **Coseismic landslides, post-seismic remobilisation of coseismic landslide deposits and post-seismic landslides (new landslides) identified from remote sensing images recorded in 2008, 2011, 2013, 2015, 2017 and 2018. For the remobilisations, the levels of activity are also indicated.**

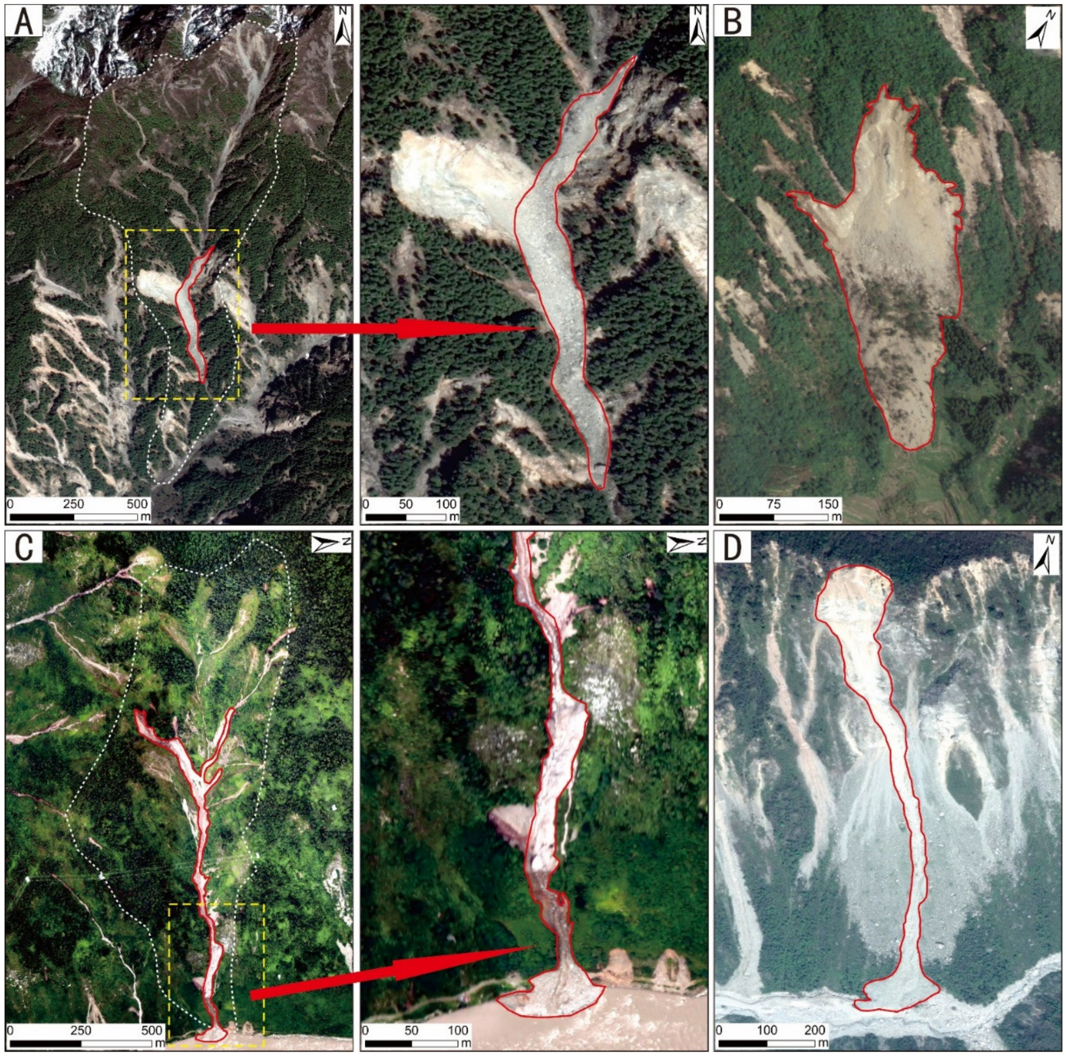

Figure 4. Types of landslides and deposits mapped in the inventory: channel deposit (A); slide (B), debris flow in a channel (C), debris flow on a hillslope (D).

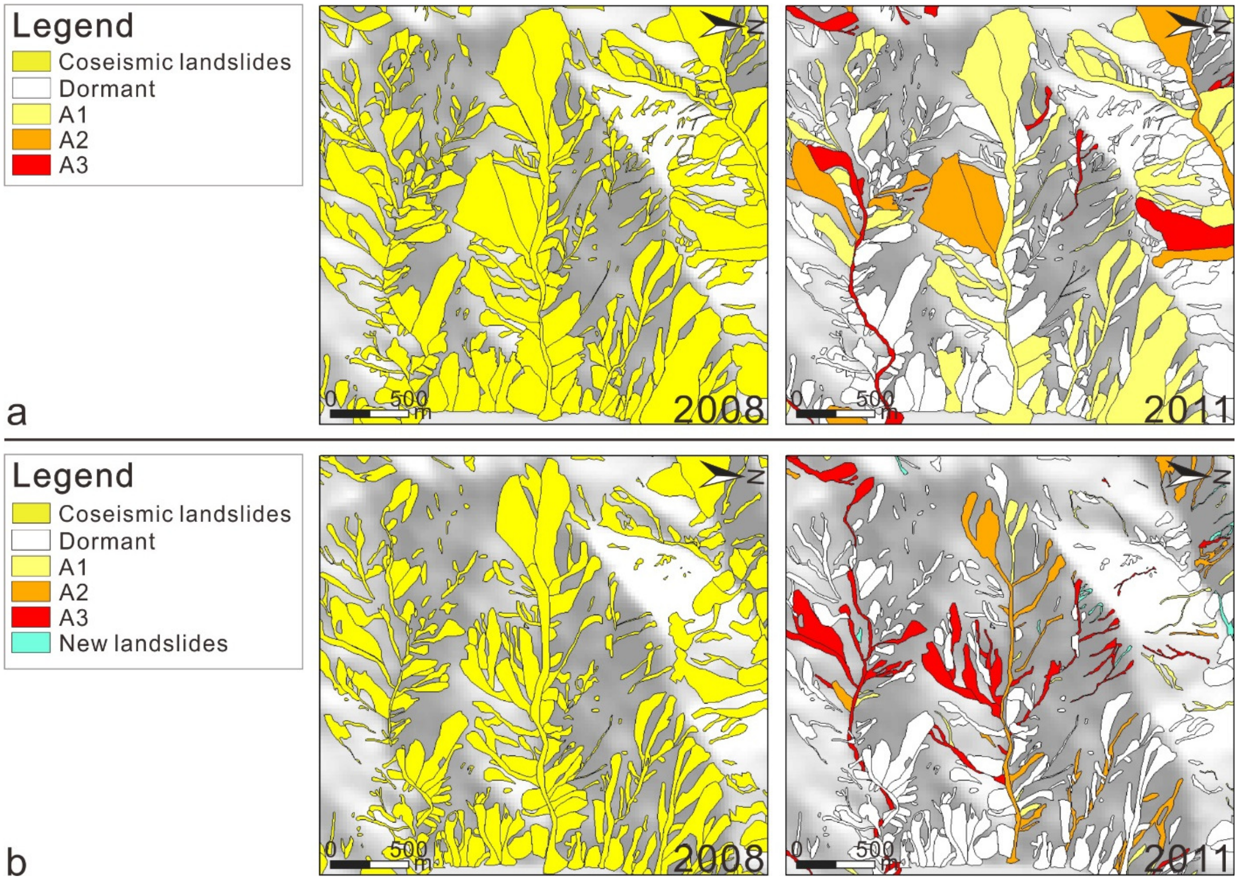

Figure 5. Comparison between the landslide mapping performed by Tang et al. (2016) and that of the present work in a portion of the study area, using the remote sensing scene recorded in 2011. Notice that Tang et al. (2016) use the polygons delineating the coseismic landslides (2008 scene) and estimate the proportion of landslide area remobilised as of 2011, providing this estimation in the attribute table of the map. Differently, in this work the remobilised areas were remapped with new polygons in each post-earthquake scene. In this way, not only the remobilised area can be calculated, but also the spatial characteristics of the remobilisations can be studied.

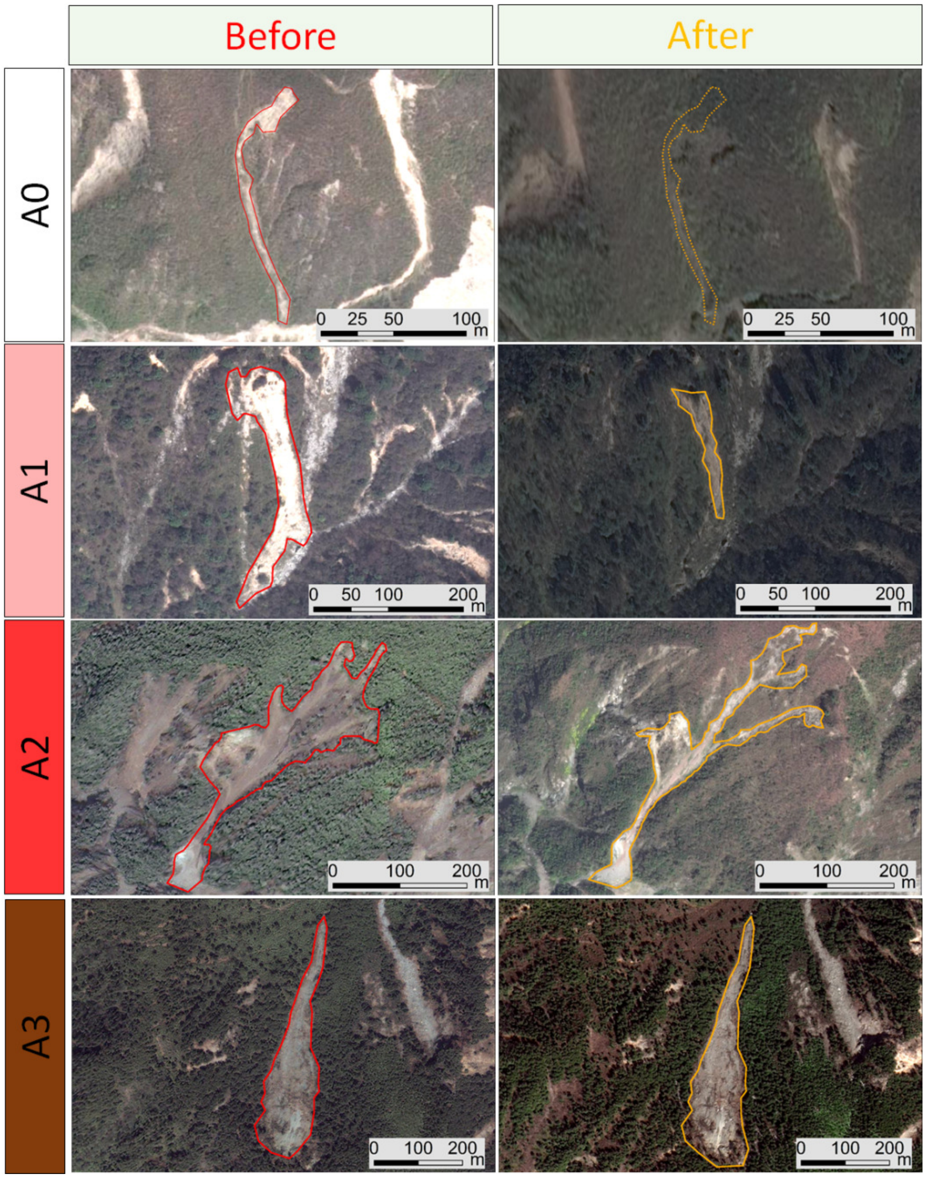

Figure 6. Examples of coseismic landslide deposits displaying different levels of activity.

3.1.2 Uncertainties

The processes of manual mapping and discernment of landslide boundaries and types are obviously affected by unavoidable uncertainties due to stochastic errors and systematic biases, such as the variable quality of the remote sensing images, and the variable experience of the mappers. Nevertheless, we still preferred this approach because, on the other hand, semi-automatic and automatic methods of landslide identification do not necessarily offer better performances, and can even lead to larger uncertainties when applied to very high resolution images (van Westen et al., 2006; Guzzetti et al., 2012; Pawłuszek et al., 2017). Moreover, some semi-automatic techniques still need visual interpretation over a significant test area for calibration (e.g., Đurić et al., 2017), and automatic methods may require a combination of images of different portions of the spectrum, or of satellite and aerial images, that should be acquired within a narrow time window to be significant for a multi-temporal inventorying of fast evolving features. Such techniques are not necessarily less time consuming than the manual interpretation (Santangelo et al., 2015).

Our mapping was carried out by five mappers who worked on distinct areas with the same set of pre-agreed rules for the identification of the landslides and their types (see also Fan et al., 2018a). The mappers worked in close contact, interacting and discussing non-easily discernible cases. Nonetheless, we evaluated the individual performances of the mappers to make an estimation of the mapping uncertainties and their propagation into further analyses. We selected a test area (a portion of a catchment), on which accurate mapping had been performed for one scene (2011), which was verified and improved during field investigation. We assumed the landslide inventory for this test area to be good enough to consider the uncertainties negligible, and we used it as a reference. We asked each mapper to produce, independently, an inventory of the same area, which we compared to the reference inventory (Figure 7). We evaluated the matching degree between each mapper's inventory and the reference inventory, M_n, which we defined as follows:

$$M_n = \frac{A_n \cap A_r}{A_r} \quad (1)$$

where A_n is the landslide area delineated by the *n-th* mapper and A_r is the respective area of the reference inventory. We then calculated the average matching degree of the team as follows:

$$M = \frac{1}{N} \sum_{n=1}^{N} M_n \quad (2)$$

where N is the number of mappers in the team. A matching degree $0.67 \leq M \leq 0.86$ was evaluated in the test area. In average, the landslide areas matched with those of the reference inventory by 76%, and an average mapping uncertainty of ±19% in terms of total landslide area was calculated. If this same value of uncertainty is assumed for the entire study area, this will be a conservative estimate, as the uncertainties will tend to decrease with the landslide areas increasing, and the test area consisted mostly of small landslides. We believe that this uncertainty can be acceptable when performing regional scale analyses, as it can be demonstrated that it does not affect the patterns of frequency-size distributions or potential controlling factors significantly (Fan et al., 2018a).

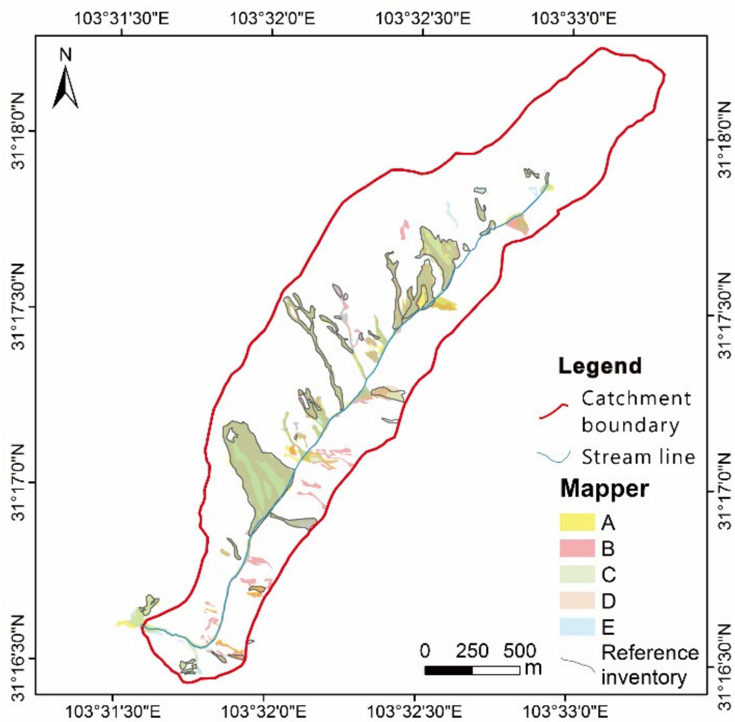

Figure 7. Landslide inventory of a test area (remote sensing image recorded in 2011): comparison between the reference, field checked inventory with those produced by five mappers (A-E) independently, on the basis of the sole imagery and a common set of rules. Darker shades indicate areas in which most inventories overlap.

3.1.3 Descriptive statistics

We identified 133 and 71 landslides on the 2005 and 2007 (pre-earthquake) scenes, respectively, and 8,917 coseismic landslides on the 2008 scene, of which 8,259 were classified as slides, 571 as debris flows and 87 as channel deposits. We also delineated 832 new landslides on the 2011 scenes (589 slides, 193 debris flows, 50 channel deposits), 387 on the 2013 scene (254 slides, 106 debris flows, 27 channel deposits), 14 on the 2015 scene (7 slides, 1 debris flow, 6 channel deposits), 5 on the 2017 scenes (2 slides, 2 debris flows, 1 channel deposit), and 9 (all slides) on the 2018 scene. On the 2011, 2013, 2015, 2017 and 2018 scenes we identified 4099, 1152, 273, 22 and 29 remobilised landslides (having levels of activity A1-A3), respectively. More details are given in Table 2. Note that some of these numbers differ from those published by Fan et al. (2018a) for the period until 2015, even though they referred to the same study area, because the inventory has been refined and improved since then.

The number of coseismic deposits that were remobilised in each period, the area affected by the remobilisation, the number and areas of new failure (i.e. the post-seismic landslides) decreased significantly over time (Table 3). The coseismic landslides covered 124 km^2; only 37 km^2 had some activity (A1-A3) in 2011, while only 14 km^2 were active in 2013, 6 km^2 in 2015, 0.27 km^2 in 2017 and 0.34 km^2 in 2018. Furthermore, the degree of activity of the coseismic deposits rapidly decreased and, with time, the number and areas of active slides decayed faster than that of debris flows. A great number of remobilisations in the form of debris flows were identified within the first three years after the earthquake (2008-2011). Then (2013-2018), the number of debris flows decreased considerably, although a large amount of coseismic material was still present on the hillslopes (Fan et al., 2018a). This suggests that the effects of the earthquake on landslide rates might be shorter than what initially expected (Huang and Fan, 2013). Some ongoing studies suggest that the changing properties of the coseismic deposits, such as in terms of grain size distribution, relative density, hydraulic conductivity, might play a key role.

The frequency-size distribution analysis (e.g., Malamud et al., 2004) carried out with the dataset (Figure 8) show the patterns of pre- and coseismic landslides and post-seismic remobilisations for the period 2005-2018. The largest number of landslides was triggered by the earthquake, while and the post-seismic rates of remobilisation decreased in the following years. This decrease mostly occurred for landslides with small areas, while the curves do not exhibit important changes in the range of landslides with large area ($A > 10^5$ m^2). The shifting of the roll over point towards higher landslide areas over time might indicate that the minimum sampling size (Malamud et al., 2004; Guzzetti et al., 2002) or the minimum area that can fail due to physical reasons (Turcotte et al., 2002) is increasing over time.

Table 2. Landslides with no information (NI), channel deposits (cd), slides (s), debris flows (d), levels of activity (A0-A3) and new landslides (NL) in the inventory.

Year	NI	cd	Activity level				NL	s	Activity level				NL	d	Activity level				NL
			A0	A1	A2	A3			A0	A1	A2	A3			A0	A1	A2	A3	
2005	133	-	-	-	-	-	-	-	-	-	-	-	-	-	-	-	-	-	-
2007	71	-	-	-	-	-	-	-	-	-	-	-	-	-	-	-	-	-	-
2008	-	87	-	-	-	-	-	8259	-	-	-	-	-	571	-	-	-	-	-
2011	-	122	12	9	11	40	50	7955	4406	860	739	1361	589	1676	404	306	332	441	193
2013	-	134	75	1	8	23	27	8799	7758	310	192	285	254	1096	657	132	107	94	106
2015	-	178	106	33	8	25	6	9016	8906	66	14	23	7	930	825	65	19	20	1
2017	-	179	178	0	0	1	1	9017	8996	6	5	8	2	932	928	0	1	1	2
2018	-	179	177	0	2	0	0	9025	8996	9	7	4	9	932	925	3	2	2	0

Table 3. Simple statistics of the landslides included in the multi-temporal inventory. Note that the volumes in this table were calculated according to the area-volume scaling proposed by Xu et al. (2016). A_{min}, A_{max}, $A_{average}$, A_{total} and V_{total} are, respectively, the minimum, maximum, average and total area of landslides, and their estimated total volume.

	A_{min} (m^2)	A_{max} (m^2)	$A_{average}$ (m^2)	A_{total} (m^2)	V_{total} (m^3)
2005	156	54 550	5 412	719 817	6 557 343
2007	1995	38 770	14 423	1 024 062	10 418 520
2008	30	584 700	13 917	124 098 226	1 466 216 338
$2011_{remobilised}$	35	348 195	8 924	36 580 002	391 925 702

2011 **new landslides**	44	514 284	5 880	4 892 221	59 776 056
2013 **remobilised**	55	461 738	12 140	13 986 239	163 382 807
2013 **new landslides**	121	473 171	8 575	3 318 339	41 095 585
2015 **remobilised**	35	372 561	21 263	5 804 788	80 229 523
2015 **new landslides**	1 672	73 974	13 303	186 240	2 043 300
2017 **remobilised**	553	70 750	12 009	264 196	2 836 643
2017 **new landslides**	3 927	27 554	10 864	43 457	430 870
2018 **remobilised**	292	62 089	11 562	335 310	3 748 479
2018 **new landslides**	228	13 911	4 141	37 273	324 802

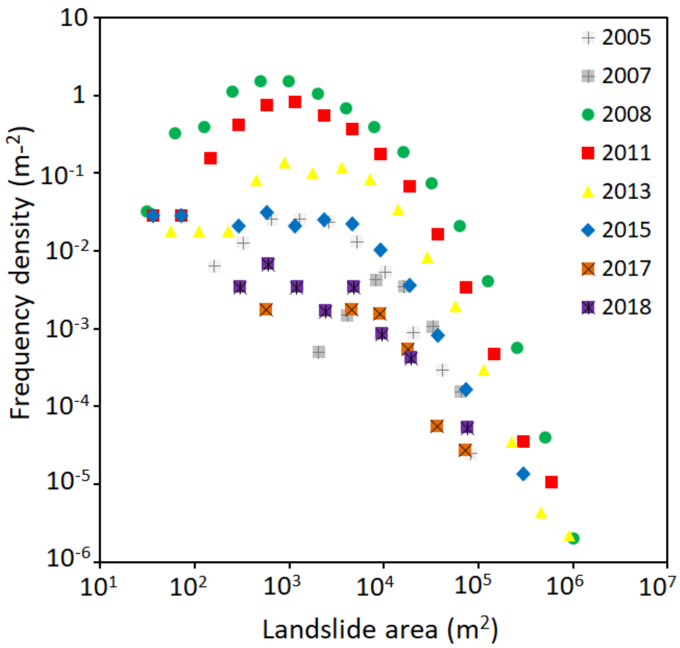

Figure 8. Frequency density – size distributions of pre-seismic landslides (2005-2007), coseismic landslides (2008) and post-seismic remobilisations (2011-2018) in the landslide inventory. Note that the amount of data in 2007, 2017 and 2018 might be insufficient to delineate clear patterns and identify a roll over point.

3.1.4 Comparison with existing inventories

Approaches to compare landslide inventory maps can entail direct or indirect comparisons (Gorum et al., 2011). The former evaluate the degree of cartographic matching between two maps through a pair-wise comparison (e.g., Galli et al., 2008), while the latter correlate the inventories through the landslide densities (e.g., Guzzetti et al., 2000), frequency-area statistics (e.g., Galli et al., 2008), or the resulting susceptibility or hazard maps (e.g., van Westen et al., 2009). Here we provide direct and indirect comparisons between our coseismic inventory and the portions of those presented by Dai et al. (2011), Xu et al. (2014) and Tang et al. (2016) that overlap with it.

The matching degrees (M, see Eq. 1) show a wide range. The worst overall match is with Dai et al. (2011)'s inventory, with M = 0.32. The match with the inventory of Xu et al. (2014) is 0.47, while the best match (M = 0.82) is obtained with the inventory of Tang et al. (2016). Notice that this matching degree is comparable to those obtained between the different mappers that produced our inventory. Through visual comparison, we can see that Dai et al. (2011) identified less landslides in our study area than we did. This might be partly explained by the lower aerial coverage of the images they used, compared to those we used. The images used by Xu et al. (2014) had comparable coverage with those we used. They identified a similar number of landslides in our study area. The mismatch with our inventory could be due to different criteria used in mapping. The matching degree has also been calculated for the other inventories. In such case, the variability is smaller as it ranges from 0.33 to 0.44, being Tang et al. (2016) vs Xu et al. (2014) the ones that show a higher correlation (M = 0.44) and Dai et al. (2011) vs Xu et al. (2014), and Tang et al. (2016) vs Dai et al. (2011) 0.34 the lowest: M = 0.33 and 0.34, respectively. These results suggest that our inventory and Tang et al. (2016)'s are the most similar ones and the one that presents the poorest correlation with the others is Dai et al. (2011)'s.

In order to verify the spatial variability of the matching degree, we repeated the analysis at catchment scale, as reported in Table 4. The missing data for Tang et al. (2016) refer to those catchments that were not covered by their inventory. The results show that our inventory and that of Tang et al. (2016) are consistently similar in the areas in which they overlap, while the matching is much less spatially consistent with respect to Dai et al. (2011) and Xu et al. (2014) inventories.

The comparison between the landslide density distributions yields the best correlation ($R^2 = 0.8154$) with the inventory performed by Tang et al. (2016). Conversely, the lowest correlation is obtained with Dai et al. (2011)'s inventory. This agrees with the result of the direct comparisons performed through the matching degree.

Finally, in Figure 10 we compare the frequency density – size distributions of the four inventories. First, we compare the results referring to the entire areas covered by each inventory (Figure 10a). Dai et al. (2011) and Xu et al. (2014) inventories exhibit higher peak values of landslide density. This can depend on the extension of the mapped area, which can include or exclude areas with little or no landsliding. It also can be noticed that the rollover points of Dai et al. (2011) and Xu et al. (2014) inventories occur in correspondence to larger landslide areas than in our inventory and that of Tang et al. (2016). This can be in part explained by the predominantly small size of the landslides in our study area compared to those of other portions of the earthquake-affected region, and in part by a possible systematic undersampling of small landslides in Dai et al. (2011) and Xu et al. (2014). Undersampling seems particularly striking in Dai et al. (2011) when the same mapped area is used as the base of comparison (Figure 10b). To a lesser extent, it can be seen also in Xu et al. (2011) for small landslide areas (less than a few hundred m^2). Our inventory and that of Tang et al. (2016) seem to suffer of undersampling with the same (possibly minimal) extent. Note also that Dai et al. (2011) show oversampling for large landslide areas, which might signal some systematic amalgamation of smaller landslide polygons.

Table 4. Matching degrees, calculated for each of the catchments delineated in our study area, between our coseismic inventory and those of Tang et al. (2016), Dai et al. (2011) and Xu et al. (2014). The catchment areas and the areas of landslides are also reported. See Figure 2 for the CID.

Catchment ID (CID)	Catchment area (km^2)	Landslide area (km^2)				Matching degree					
		this work	Tang et al. (2016)	Dai et al. (2011)	Xu et al. (2014)	our work with Tang et al. (2016)	our work with Dai et al. (2011)	our work with Xu et al. (2014)	Tang with Dai	Tang with Xu	Dai with XU
1	28.59	10.02	-	4.78	8.55	-	0.26	0.48	-	-	0.37
2	7.25	2.48	-	1.40	1.90688	-	0.32	0.40	-	-	0.56
3	24.53	8.66	-	4.28	9	-	0.26	0.50	-	-	0.25
4	7.37	3.32	0.81	1.26	3.72125	0.17	0.23	0.61	0.90	0.13	-
5	4.12	0.83	0.65	0.51	0.5975	0.61	0.24	0.27	0.33	0.31	-
7	39.78	7.59	6.91	5.34	10.9288	0.56	0.29	0.45	0.63	0.31	-
8	3.80	0.75	0.71	-	0.504375	0.59	-	0.17	-	0.25	-
9	3.48	0.40	0.64	-	0.613125	0.70	-	0.40	-	0.42	-
10	3.60	0.45	0.66	-	0.5475	0.81	-	0.36	-	0.43	-
11	3.91	0.71	0.70	-	0.663125	0.55	-	0.25	-	0.27	-
12	2.26	0.43	0.56	-	0.495	0.74	-	0.37	-	0.44	-
13	5.93	0.71	0.84	-	0.83875	0.82	-	0.31	-	0.31	-
14	6.61	1.01	1.10	0.47	0.9125	0.77	0.27	0.38	0.32	0.48	0.49
15	1.87	1.58	1.37	0.83	1.03688	0.92	0.45	0.58	0.71	0.88	0.68
16	6.72	2.75	3.16	2.63	2.545	0.82	0.47	0.48	0.79	0.65	0.62
17	8.11	3.05	4.03	2.57	2.82688	0.87	0.40	0.42	0.59	0.65	0.45
18	5.59	2.66	1.57	1.73	2.42188	0.49	0.46	0.62	0.57	0.43	0.48
19	4.02	2.32	2.87	2.14	2.1	0.95	0.62	0.60	0.90	0.86	0.66
20	7.79	3.59	-	2.96	3.08813	-	0.50	0.56	-	-	0.61
21	23.83	5.30	-	3.90	10.4331	-	0.49	0.60	-	-	0.26
22	2.62	1.40	0.96	1.01	1.32813	0.61	0.48	0.58	0.83	0.52	0.67
23	7.09	2.42	2.75	1.78	1.91875	0.90	0.34	0.36	0.53	0.55	0.46
24	2.39	1.07	0.90	0.81	0.7225	0.86	0.43	0.36	0.78	0.55	0.69
25	5.94	1.86	2.18	1.20	1.845	0.87	0.31	0.46	0.48	0.59	0.46
26	8.55	2.35	2.58	-	2.13188	0.90	-	0.35	-	0.47	-
27	4.84	0.96	0.93	0.06	0.913125	0.66	0.00	0.30	0.00	0.37	0.02
28	4.44	0.20	0.31	-	0.33	0.69	-	0.33	-	0.24	-
29	13.31	3.87	2.03	2.57	3.67125	0.37	0.31	0.42	0.64	0.26	0.38
30	13.91	5.17	-	1.30	3.20438	-	0.15	0.38	-	-	0.22
35	4.04	2.35	1.67	1.53	1.34375	0.90	0.63	0.55	0.93	0.71	0.73
48	50.91	9.17	-	5.18	12.5238	-	0.19	0.46	-	-	0.21
59	15.76	0.65	-	0.39	0.485625	-	0.30	0.43	-	-	0.63
60	5.53	0.78	-	0.70	1.05125	-	0.28	0.45	-	-	0.44

65	17.60	5.12	-	2.81	5.36375	-	0.28	0.50	-	-	0.35
66	4.48	2.40	-	2.68	2.54938	-	0.71	0.66	-	-	0.77
67	6.70	2.32	2.41	1.26	1.94313	0.86	0.27	0.39	0.41	0.53	0.45
68	6.87	1.38	-	1.31	1.9125	-	0.30	0.50	-	-	0.33
69	10.38	0.81	-	0.81	1.795	-	0.22	0.46	-	-	0.21
70	21.72	5.40	-	4.15	6.30563	-	0.30	0.46	-	-	0.36
71	4.81	0.53	0.70	0.34	0.838125	0.45	0.25	0.36	0.26	0.24	0.33
72	26.31	8.51	5.94	5.75	6.78875	0.67	0.41	0.42	0.66	0.42	0.51
73	33.68	5.45	-	5.14	11.6181	-	0.38	0.61	-	-	0.25
Total	***471.01***	***122.81***	***49.4***	***75.58***	***134.32***	***0.82***	***0.32***	***0.47***	***0.34***	***0.44***	***0.33***

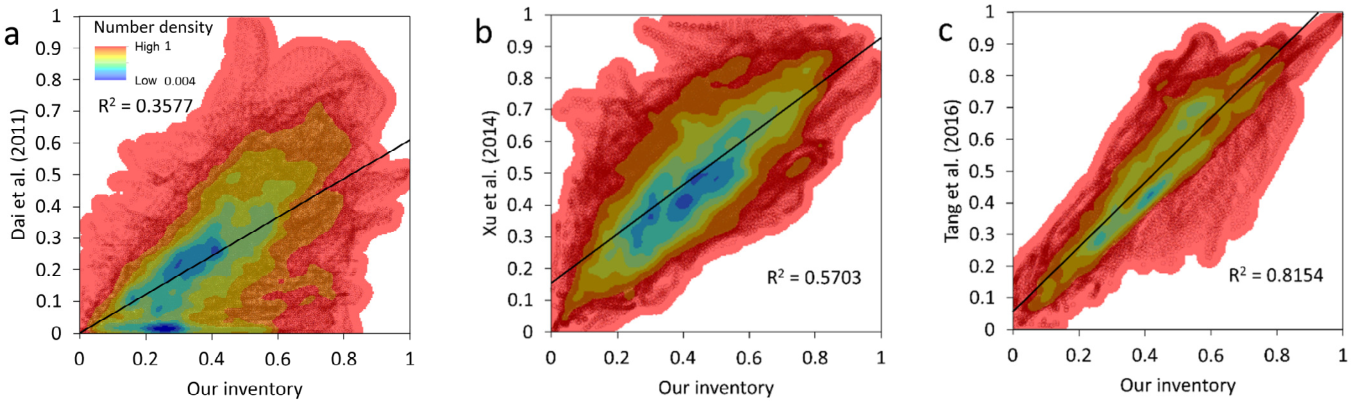

Figure 9. Pixel-based spatial correlation of landslide densities. The comparisons between our inventory map and those obtained by Dai et al. (2011) (a), Xu et al. (2014) (b) and Tang et al. (2016) (c) are shown.

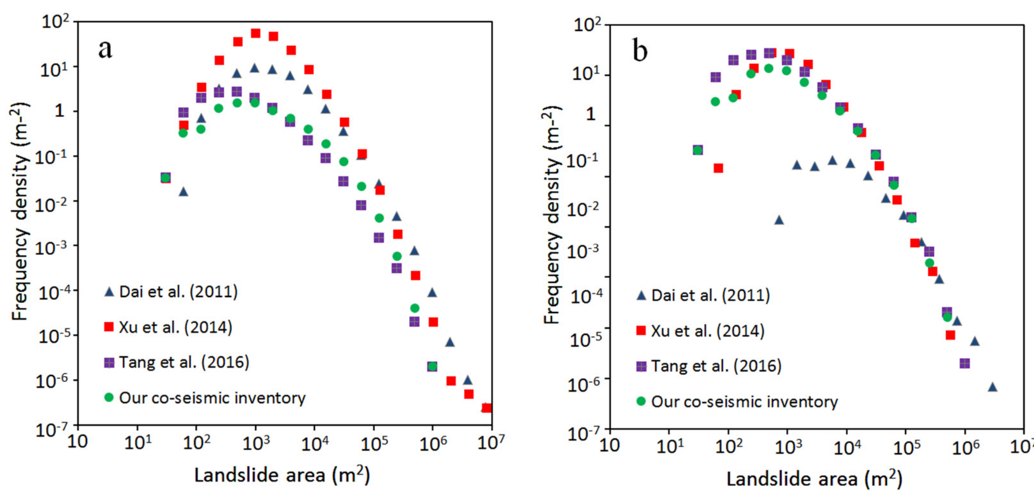

Figure 10. Comparison of the frequency density – size distributions of the coseismic landslides mapped in the Wenchuan earthquake-affected area by Dai et al. (2011), Xu et al. (2014) and Tang et al. (2016). The relationship refers to the whole extension of each inventory in (a) and is limited to the area which is common to all the inventories in (b), i.e. the area mapped by Tang et al. (2016).

For further comparison, we estimated the volume of the coseismic landslides through a set of empirical area-volume scaling relationships from the literature (Guzzetti et al., 2009; Larsen et al., 2010; Parker et al., 2011; Xu et al., 2016). These relationships provide a quick, first-order estimation of the landslide volumes from the mapped landslide areas. They were calibrated by their authors in different ways (i.e. using landslide depths measured in the field or differential DEM techniques on datasets of different sizes). Guzzetti et al. (2009) calibrated their relationship using data from 677 landslides of the slide type, with areas ranging from 2 m^2 to 10^9 m^2; Larsen et al. (2010) employed a dataset of 4,231 landslides, comprising soil and bedrock failures ranging from 1 m^2 to 10^7 m^2; Parker et al. (2011) used field measurements of 41 coseismic landslides triggered by the 2008 Wenchuan earthquake but they did not provide information on the sizes of these landslides; Xu et al. (2016) used both field observations and remote sensing analyses of 1,415 coseismic landslides triggered by the 2008 Wenchuan earthquake, all having sizes exceeding 10^4 m^2.

These empirical relationships are expressed using a power law in the form: $V = \alpha \cdot A^{\gamma}$, where V is the individual landslide volume, A is the mapped individual landslide area, and α and γ are calibrated parameters. A higher value of γ underlies an abundance of deep bedrock landslides in the calibration dataset, while lower values of γ are more representative of shallow landslides, as discussed by Parker et al. (2011). The relationships, with the uncertainties (±1σ) on the calibrated parameters, as given by the respective authors, read as follows: $V = 0.074 \cdot A^{1.450 \pm 0.009}$ (Guzzetti et al., 2009); $V = (0.146 \pm 0.005) \cdot A^{1.332 \pm 0.005}$ (Larsen et al., 2010); $V = 0.106 \cdot A^{1.388 \pm 0.087}$ (Parker et al., 2011); and $V = 1.3147 \cdot A^{1.2085 \pm 0.0131}$ (Xu et al., 2016).

The total landslide volume is, obviously, the sum of the individually computed landslide volumes. As noted by Parker et al. (2011), if the inventory includes amalgamated landslide polygons, there will be a systematic overestimation of the total volume. For our mapping, we are confident, also in the light of the comparisons presented in Figure 10, that the incidence of amalgamation is limited, as the polygon-based mapping was performed by visual interpretation with field-checking on high-resolution images, rather than by semi-automatic mapping techniques, which have been shown to be more susceptible to this kind of mapping error (e.g. Marc and Hovius, 2005). The results of the calculations using the various empirical relations applied to the various inventories are reported in Table 5, with reference to the area that is common to all the inventories (which corresponds to the area mapped by Tang et al., 2016). Note that the relationship by Larsen et al. (2010) consistently yields the smallest volumes for all the inventories, while the largest volumes are obtained either through Guzzetti et al. (2009) or Xu et al. (2016) relationships, depending on the inventory. Also note that, in the given study area, depending on the inventory map and the scaling relationship, volumes in a wide range (174-630 x 10^6 m^3) can be estimated, to which the uncertainties on the scaling parameters and on the landslide boundaries also should to be added. If the former are considered (in the form of

±1σ, see Table 5), the volume range will span over one order of magnitude (92-1153 x 10^6 m^3). Quantifying the latter is more difficult, but has been attempted for our inventory (see Section 3.1.2, Figure 7, and Fan et al., 2018a).

Table 5. Comparison between the total volumes of coseismic landslides in the portion of the Wenchuan earthquake-affected area that was covered by all the inventories (i.e. our inventory and those of Dai et al., 2011; Xu et al., 2014; Tang et al. 2016), estimated through area-volume empirical relationships (Guzzetti et al., 2009; Larsen et al., 2014; Parker et al., 2011; Xu et al., 2016). The first value in each cell is the central value, while those in brackets result from the uncertainty (±1σ) of the calibrated parameters of the relationships.

Inventory	Area volume empirical relationship (x 10^6 m^3)			
	(Guzzetti et al., 2009)	(Larsen et al., 2010)	(Parker et al., 2011)	(Xu et al., 2016)
Our inventory	390 (353-430)	215 (197-235)	285 (112-733)	521 (454-598)
Dai et al. (2011)	583 (519-655)	255 (232-281)	377 (125-1153)	490 (417-577)
Xu et al. (2014)	305 (277-335)	174 (160-190)	227 (92-569)	444 (389-506)
Tang et al. (2016)	484 (439-535)	263 (241-287)	351 (137-914)	630 (549-724)

3.2 Inventory of debris flows and their triggering rainfalls

3.2.1 Data acquisition, structure of the dataset and attributes

We compiled a dataset of debris flows from the existing literature which occurred after the 2008 Wenchuan earthquake until the rainy season in summer 2017. These events are associated to the recordings of rain gauges and are spread over an area of 16,959 km^2.

The structure of the dataset is summarised in Table 4. The dataset contains information on the locations, date and time of occurrence of debris flows, and on the rainfalls that triggered them. We included data not only for catastrophic and well-studied events (e.g., Tang et al., 2012; Xu et al., 2012), but also for smaller events that did not cause fatalities or heavy damage to the population and the infrastructure, but had sufficient runout to approach or reach the catchment outlet. The material of these events can come from different slides, hillslope and channelized debris flows and, mainly, from the existing channel deposits material, all of them presented in the multi-temporal inventory of landslides (Sections 2.1 and 3.1). We used a 25-m resolution digital elevation model, provided by the Sichuan Bureau of Surveying and Mapping, to define the catchment boundaries. The rainfall data were obtained from the Meteorological Administration of China, from the Meteorological Bureau of Sichuan Province, from the bureau of land and resources of Chengdu and from the WebGIS monitoring network of the State Key Laboratory of Geohazard Prevention and Geoenvironment Protection (SKLGP, Chengdu, China; see Huang et al., 2015). These data were all recorded by automatic rain gauges.

We verified most of the debris flows included in the dataset by reviewing 76 published works (see file named “References of data sources” in the repository). For the largest and most catastrophic events, we performed field investigations and interviews to the local residents with a minimum of two surveyors. There is no fixed period of the year during which field inspections were carried out, as they mostly followed the occurrence of strong rainfalls. We also collected information from the monitoring system that the SKLGP implemented in some catchments (see Figure 1). The debris flows were georeferenced through the latitude and longitude of the outlet of the catchment in which they occurred. Information on the rainfall that triggered each debris flow is provided for the rain gauges located in closest proximity to them (< 5 km). In case no rain gauges were actively recording within this distance, data from the closest rain gauge are provided. There are 391 of 527 debris flow-affected catchments with rain gauges within 5 km from the locations of the catchment outlets. We chose to provide rainfall data with the highest resolution available (in most cases hourly rainfall, in some cases 10-minutes rainfall) for a time window starting from one week before until one day after the debris flow event. The choice of this window should allow for the inclusion of the significant antecedent rainfall in our setting that can be used for further analyses of the triggering conditions of the debris flows. If the reader requires them, rainfall series with wider time windows can be obtained from the authors upon request.

For one catchment (Er catchment; No. 1 in Figure 1b; Table 5; Cui et al., 2018), we release data series of rainfall intensity, flow discharge, density and height. The Er catchment is administratively part of Yingxiu township and covers 39.4 km^2 with a channel length of 11.5 km. The Ergou River flows within the catchment, which is a tributary of the Minjiang River. The headwater elevation of the catchments is 4,120 m a.s.l. and the outlet is located at 990 m a.s.l. Rainfall intensity was obtained through rain gauges with 0.5-mm tipping buckets. Flow discharge was calculated as the product of the cross-sectional mean velocity and the cross-sectional area of the flow. The latter was calculated from the depth, obtained from the data measured by the ultrasonic stage meter, in combination with the detailed geometry of each section. The surface velocity of the flow was measured using automatic radar speed indicators and compared with video images (Yan et al., 2016). As flow velocity varies with depth, the relationship obtained by Takahashi (1991) was used. Flow depths were measured using ultrasonic stage meters TSS908, Beijing Guda instrument Co., Ltd.), with 1-min recording frequency, 0–30 m measurement range and ±10 mm error. For additional information, the reader is referred to Cui et al. (2018). For other well-monitored catchments (No. 2, 3 and 4 in Figure 1b), we release rainfall data for three important debris flow events (see Section 3.2.3, below), while full data series are available from the authors upon request.

Table 6. Structure of the dataset of debris flows and their triggering rainfalls. An additional shape file is provided to define the catchment boundaries with a simple characterisation (CID, catchment name and county, gradient and internal relief, drainage density and channel length).

Folder name	File name	File type	Layers/sheets	Attributes (columns)
DF_RG_inventory	DF_RG_inventory	Shape file (.shp) and spreadsheet (.xls)	debris_flows	DF_ID, CID, Gully_name, Latitude, Longitude, Year, Month, Day, Time_24h_, T_Comment, Source_vol, Depo_vol, List_of_RG, Monitoring, Number of Dams, Reference

			rain_gauges	RG_ID, CID, coordinates, temporal resolution, units, data references
R_DF_ID_X*	A_B_CDEF	Spreadsheet (.xls)	-	date and time, amount of rain

Attributes: DF_ID: identifier of the debris flow; CID: identifier of the catchment to which the debris flow or the rain gauge belong; Gully_name: name of the catchment; Latitude: latitude of the debris flow event (º); Longitude: longitude of the debris flow event (º); Year: year the debris flow event occurred; Month: month the debris flow event occurred; Day: day the debris flow event occurred; Time_24h_: time at which the debris flow occurred (24 h); T_Comment: specifications on the time of occurrence of the debris flow (initiation, deposition or range of days); Source_vol: available material during the initiation of the debris flow (m^3); Depo_vol: volume of debris flow deposited at the fan area (m^3); List_of_RG: list of rain gauges (identifier) located in proximity to the debris flow event that were actively recording throughout the time window of interest for that debris flow; Monitoring: specifies if additional monitoring data are available for that event (Y: yes; N: no); Number of Dams: specifies the number of dams built in each catchment as mitigation measures; References: source of each debris flow event.

* one folder for each debris flow event being "X" the debris flow event identifier (DF_ID). Each folder contains the rain gauges located within a distance of 5 km for a given event. "A" indicates the relative position of each rain gauge from the debris flow event in ascending order; "B" refers to the rain gauge identifier (RG_ID); C, D and E indicate the year, month and day of the debris flow event, respectively, and F refers to the starting time of the rain. Rain is expressed in mm. Each spreadsheet provides data from 7 days before to one day after the date associated with the debris flow event (DF_ID). Full data series are available, from the authors upon request, for further analysis.

Table 7. Released information on some well-monitored catchments.

File name	File type	Sheets	Attributes (columns)
Er_vel_rain_disc_dens	Spreadsheet (.xls)	debris_flows	Latitude and Longitude of each station (º), Rainfall intensity measured at R1 (mm/h); Discharge measured at S1, S2 and S3 (m^3/s); Flow density measured at S1 (g/cm^3) and Flow depth (m) vs flow velocity (m/s) measured at S1 (Peng et al., 2018)
Rainfall distribution	Spreadsheet (.xls)	Qingping_a	Rain gauge coordinates, Date, Daily rainfall (mm), Cumulative rainfall (mm) (You et al., 2018)
		Qingping_b	Rain gauge coordinates, Date, Time (h), Hourly rainfall (mm), Cumulative rainfall (mm) (You et al., 2018).
		Hongchun	Rain gauge coordinates, Date, Time (h), Hourly rainfall (mm), Cumulative rainfall (mm) (Tang et al., 2011)
		Er	Rain gauge coordinates, Date, Time (h), Hourly rainfall (mm), Cumulative rainfall (mm) (Cui et al., 2018)

3.2.2 Uncertainties

Especially for minor debris flows, the time of debris flow occurrence may be uncertain, especially in those locations that lack proper instrumentation or eyewitnesses. Moreover, ambiguities in the definition of this time, as the debris flow has a finite duration, may occur. In this work, the time refers to the arrival of the flow at the outlet of the catchment, unless otherwise stated.

Rainfall recordings from rain gauges located within or near a catchment in which a debris flow developed are not equally representative of the rainfall that actually triggered the debris flow and permitted its runout. In our dataset we decided to be inclusive by using a wide buffer around the event location, not to discard some data series that may be useful for analyses of rainfall variability at local scale and to perform interpolations. However, it is worth reminding that the spatio-temporal patterns of rainfalls in mountainous areas can be extremely inhomogeneous (e.g., Nikolopoulos et al., 2014). Significant variations may exist even within the same catchment, over distances of a few km or even just a few hundreds of metres (e.g., Smith et al., 2003; Panziera et al., 2011), in dependence, for instance, on the variability of the elevation, slope and aspect of the area, in combination with the local pattern of wind at the time of the rain event. Moreover, rain gauges are usually installed in valleys and channels, while debris flows originate high on the slopes (Stoffel et al., 2011), which can generate a systematic bias. The uncertainties that derive from imperfect choices of the representative rain gauge(s) for a debris flow event have been shown to lead to large underestimations of the debris flow-triggering thresholds and to strongly limit the performance of warning systems (Nikolopoulos et al., 2014; Guo et al., 2016, 2017). Therefore, these uncertainties should be carefully estimated and minimised with appropriate strategies whenever possible. Various studies, for instance, suggested the use of weather radar and satellite-based rainfall estimates to assess the representative rainfalls for debris flows (Kirschbaum et al., 2012; Rossi et al., 2012), but the literature featuring methods to address the issue of rainfall variability systematically is still poor (Guzzetti et al., 2007; Jakob et al., 2012).

3.2.3 Descriptive statistics

The dataset contains information about 527 debris flows which occurred in 244 catchments, and rainfall data from 91 rain gauges. Most of the debris flows occurred during the summertime heavy rainfalls of 2008, 2010 and 2013, particularly in the counties of Wenchuan and Beichuan (Table 6).

In Figure 11, examples of rainfall data series are reported for well-monitored debris flow events in Qingping, Hongchun and Er catchments (see Table 5). In Figures 12 and 13, the well-monitored debris flow event in Er catchment is shown (photographs, rainfall data, flow discharge, height and density).

Table 8. Simple statistics of the debris flows and their triggering rainfalls recorded in the dataset.

By year	
Year	**No. of debris flows**
2008	195
2009	25
2010	167
2011	36
2012	29

By location		
Location	**No. of debris flows**	**No. of catchments**
Wenchuan	167	67
Pengzhou	43	23
Mianzhu	92	26
Anxian	40	11

2013	68
2014	3
2015	1
2016	2
2017	1

Beichuan	185	117

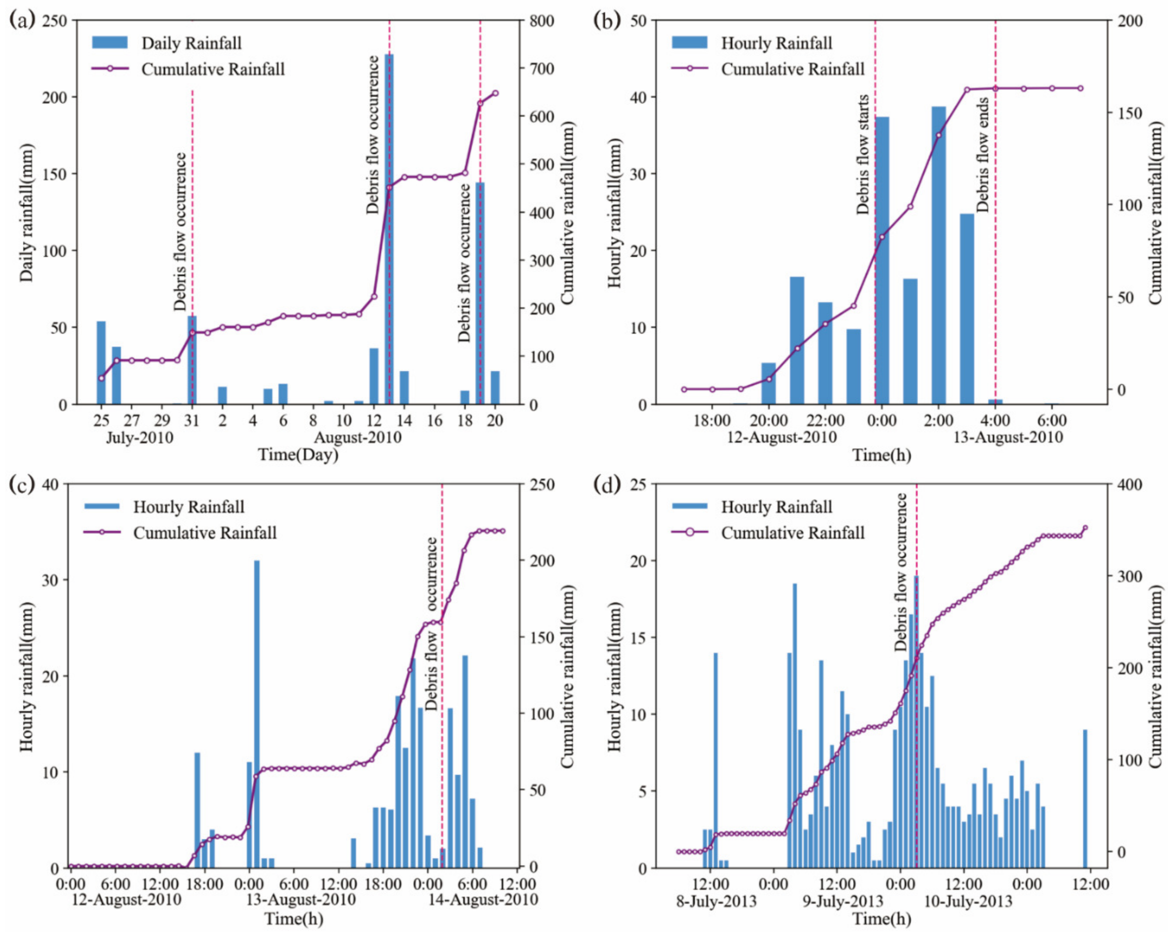

Figure 11. (a) Daily and accumulated precipitation in Qingping (Wenjia gully, CID M9, Mianzhu County; No. 4 in Figure 1c) during a period affected by the three debris flow events. The DF_ID of these events are, chronologically, 272, 302 and 273. Rainfall data were recorded by a rain gauge located in Nanmu (CID M22, LAT 104.154533, LONG 31.48832, Yu et al., 2010). (b) Detail of the second debris flow (DF_ID 302) occurred between 12 and 13 August 2010 in Qingping: hourly and accumulated precipitations and event start and end are represented. (c) Hourly and accumulated precipitation in Hongchun (CID W25, Wenchuan County; No. 2 in Figure 1c). A debris flow occurred on 14 August 2010 (DF_ID 53). Rainfall data were recorded by a rainfall gauge located in Yingxiu (LAT 103.4826; LONG 31.06417). (d) Hourly and accumulated precipitation in Er (CID W7, Wenchuan County; No. 1 in

Figure 1c). A debris flow occurred on 10 July 2013 (DF_ID 164). Rainfall data were recorded by a rainfall gauge located in Er (LAT 103.46088; LONG 31.11679; R1 in Figure 13a; Cui et al., 2018).

Figure 12. Debris flow event recorded in Er (CID W7, Wenchuan County; No. 1 in Figure 1c) on 5 July 2016 (Cui et al., 2018).

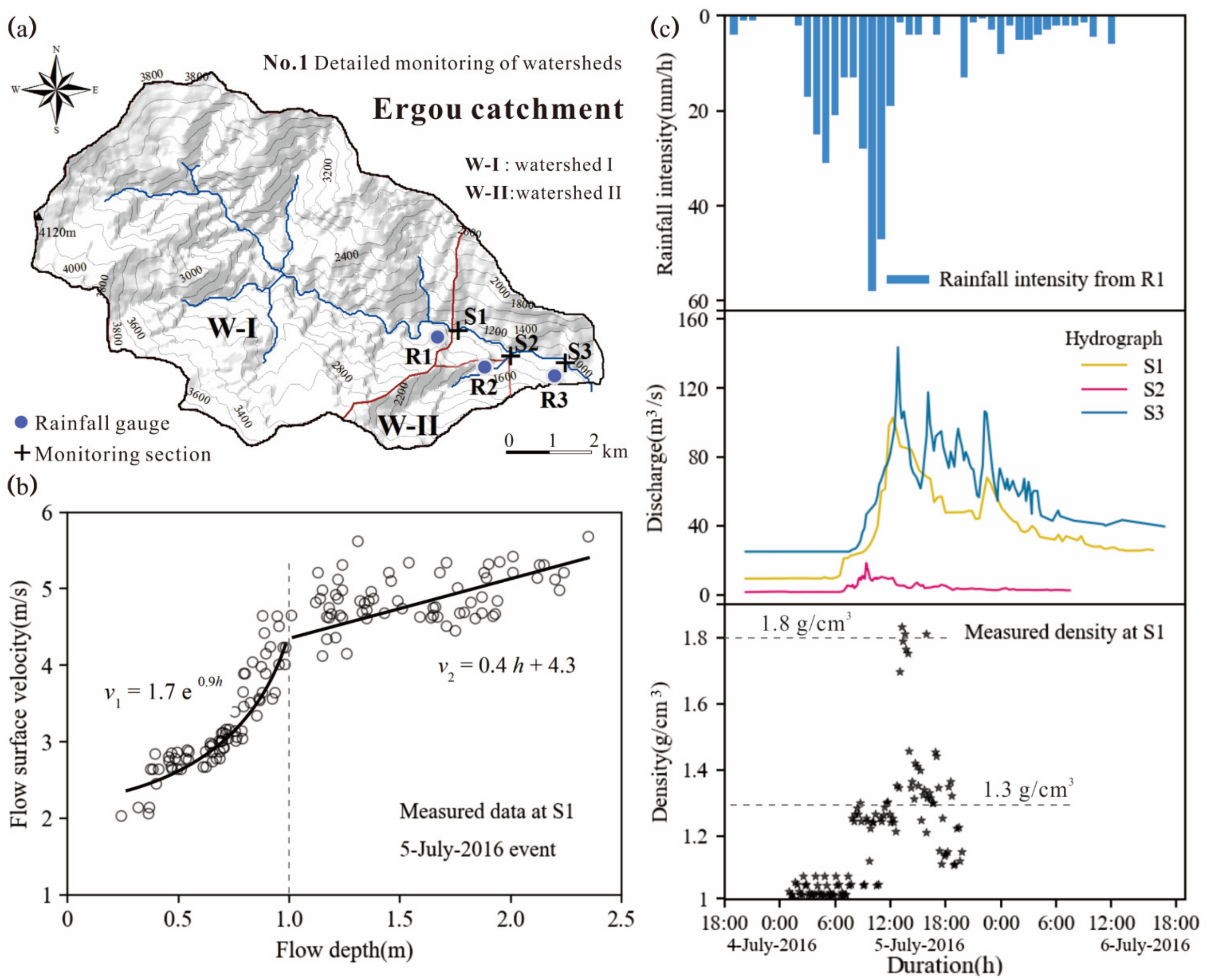

Figure 13. Data analysis of the debris flow which occurred on 5 July 2016 (Figure 12) in Er (CID W7, Wenchuan County; No. 1 in Figure 1c; Cui et al., 2018). (a) Map of the catchment; (b) Flow surface velocity vs flow depth; (c) rainfall intensity, flow discharge and flow density.

4 Data availability

The datasets are freely downloadable from https://doi.org/10.5281/zenodo.1405489 (Domènech et al., 2018). In addition to the data, the repository contains supplementary material (metadata files) that clarify the structures of the datasets, and a reference list for the data sources.

5 Summary

We presented a multi-temporal inventory of landslides in a portion of the area affected by the 2008 Wenchuan earthquake covering the period from 2005 to 2018 and an inventory of debris flows and their triggering rainfalls over a larger area covering the period from 2008 to 2017. The two datasets, which are freely available, can provide an insight into the spatial and temporal patterns of the enhanced mass wasting caused by a strong earthquake. We encourage other researchers to follow our example by sharing analogous datasets, to build an open collection of data and facilitate meta-analyses among multi-temporal datasets of mass wasting induced by earthquakes or other triggers.

6 Author contributions

XF designed the work, together with GD and GS; GS wrote the manuscript; GD, LD and FY compiled the datasets and prepared the display items; GD, LD, and FY performed the mapping supervised by XF; XG and CH provided some of the data, and suggestions on some methods; XF, RH and QX acquired project funds and supervised the project; all authors revised and approved the datasets and the manuscript.

7 Competing interests

The authors declare that they have no competing interests.

8 Acknowledgements

The collection and processing of the data presented in this paper were funded by National Science Fund for Excellent Young Scholars of China (Grant No. 41622206), the Funds for Creative Research Groups of China (Grant No. 41521002), the Fund for International Cooperation (NSFC-RCUK_NERC), Resilience to Earthquake-induced landslide risk in China (grant No. 41661134010). We also want to thank the contribution of all the group of experts during the mapping.

References

Broeckx, J., Vanmaercke, M., Duchateau, R., and Poesen, J.: A data-based landslide susceptibility map of Africa, Earth Sci. Rev., 185, 102-121, doi: 10.1016/j.earscirev.2018.05.002, 2018.

Corominas, J., van Westen, C., Frattini, P., Cascini, L., Malet, J. P., Fotopoulou, S., Catani, F., Van Den Eeckhaut, M., Mavrouli, O., Agliardi, F., Pitilakis, K., Winter, M. G., Pastor, M., Ferlisi, S., Tofani, V., Hervás, J. and Smith, J. T.: Recommendations for the quantitative analysis of landslide risk. Bull. Eng. Geol. Environ., 73, 209-263, 2014.

Cui, P., Wei, F. Q., He, S. M., You, Y., Chen, X. Q., Li, Z. L., and Yang, C.L.: Mountain disasters induced by the earthquake of May 12 in Wenchuan and the disasters mitigation. J. Mt. Sci., 26 (3), 280–282, 2008.

Cui, P., Chen, X. Q., Zhu, Y. Y., Su, F. H., Wei, F. Q., Han, Y. S., Liu, H. J., and Zhuang, J. Q.: The Wenchuan Earthquake (May 12, 2008), Sichuan Province, China, and resulting geohazards. Nat. Hazards, 56 (1), 19–36, doi: 10.1007/s11069-009-9392-1, 2011.

Cui, P., Guo, X., Yan, Y., Li, Y., and Ge, Y.: Real-time observation of an active debris flow watershed in the Wenchuan Earthquake area, doi: 10.1016/j.geomorph.2018.08.024, 2018.

Dadson, S. J., Hovius, N., Chen, H., Dade, W. B., Lin, J. C., Hsu, M. L., Lin, C. W., Horng, M. J., Chen, T. C., Milliman, J., and Stark, C. P.: Earthquake-triggered increase in sediment delivery from an active mountain belt, Geology, 32 (8), 733-736, doi: 10.1130/G20639.1, 2004.

Dai, F. C., Xu, X., Yao, X., Xu, L., Tu, X. B., and Gong, Q. M.: Spatial distribution of landslides triggered by the 2008 Ms 8.0 Wenchuan earthquake, China, J. Asian. Earth Sci., 40, 883-895, doi: 10.1016/j.jseaes.2010.04.010, 2011.

Ding, H., Li, Y., Ni, S., Ma, G., Shi, Z., Zhao, G., Yan, L., and Yan, Z.: Increased sediment discharge driven by heavy rainfall after Wenchuan earthquake: A case study in the upper reaches of the Min River, Sichuan, China, Quatern. Int., 333, 122-129, doi: 10.1016/j.quaint.2014.01.019, 2014.

Domènech, G., Yang, F., Guo, X., Fan, X., Scaringi, G., Dai, L., He, C., Xu, Q., Huang, R.: Two multi-temporal datasets to track the enhanced landsliding after the 2008 Wenchuan earthquake, version 2, Zenodo repository, doi: 10.5281/zenodo.1405489, 2018.

Durić, D., Mladenović, A., Pešić-Georgiadis, M., Marianović, M., and Abolmasov, B.: Using multiresolution and multitemporal satellite data for post-disaster landslide inventory in the Republic of Serbia, Landslides, 14, 1467-1482, doi: 10.1007/s10346-017-0847-2, 2017.

Fan, X., van Westen, C. J., Korup, O., Görüm, T., Xu, Q., Dai, F., Huang, R., and Wang, G.: Transient water and sediment storage of the decaying landslide dams induced by the 2008 Wenchuan earthquake, China, Geomorphology, 171–172, 58-68, doi: 10.1016/j.geomorph.2012.05.003, 2012.

Fan, X., Xu, Q., Scaringi, G., et al.: Failure mechanism and kinematics of the deadly June 24th 2017 Xinmo landslide, Maoxian, Sichuan, China, Landslides, 14 (6), 2129-2146, doi: 10.1007/s10346-017-0907-7, 2017a.

Fan, X., Xu, Q., van Westen, C. J., Huang, R., and Tang, R.: Characteristics and classification of landslide dams associated with the 2008 Wenchuan earthquake, Geoenvironmental Disasters, 4, 12, doi: 10.1186/s40677-017-0079-8, 2017b.

Fan, X., Domènech, G., Scaringi, G., Huang, R., Xu, Q., Hales, T. C., Dai, L., Yang, Q., and Francis, O.: Spatio-temporal evolution of mass wasting after the 2008 Mw 7.9 Wenchuan Earthquake revealed by a detailed multi-temporal inventory, Landslides, doi: 10.1007/s10346-018-1054-5, 2018a.

Fan, X., Juang, C. H., Wasowski, J., Huang, R., Xu, Q., Scaringi, G., van Westen, C. J., and Havenith, H. B.: What we have learned from the 2008 Wenchuan Earthquake and its aftermath: A decade of research and challenges, Eng. Geol., 241, 25-32, doi: 10.1016/j.enggeo.2018.05.004, 2018b.

Fan, X., Scaringi, G., Xu, Q., Zhan, W., Dai, L., Li, Y., Pei, X., Yang, Q., and Huang, R.: Coseismic landslides triggered by the 8th August 2017 Ms 7.0 Jiuzhaigou earthquake (Sichuan, China): factors controlling their spatial distribution and implications for the seismogenic blind fault identification, Landslides, 15 (5), 967-983, doi: 10.1007/s10346-018-0960-x, 2018c

Fan, X., Xu, Q., and Scaringi, G.: Brief communication: Post-seismic landslides, the tough lesson of a catastrophe, Nat. Hazards Earth Syst. Sci, 18 (1), 393-403, doi: 10.5194/nhess-18-397-2018, 2018d.

Galli, M., Ardizzone, F., Cardinali, M., Guzzetti, F., and Reichenbach, P.: Comparing landslide inventory maps, Geomorphology, 94 (3-4), 268-289, doi: 10.1016/j.geomorph.2006.09.023, 2008.

Gariano, S. L., and Guzzetti, F.: Landslides in a changing climate, Earth Sci. Rev., 162, 227-252, doi: 10.1016/j.earscirev.2016.08.011, 2016.

Gorum, T., Fan, X., van Westen, C. J., Huang, R., Xu, Q., Tang, C., and Wang G.: Distribution pattern of earthquake-induced landslides triggered by the 12 May 2008 Wenchuan earthquake, Geomorphology, 133, 152–167, doi: 10.1016/j.geomorph.2010.12.030, 2011.

Guo, X., Cui, P., Li, Y., Ma, L., Ge, Y., and Mahoney, W. B.: Intensity-duration threshold of rainfall-triggered debris flows in the Wenchuan Earthquake affected area, China, Geomorphology, 253, 208–216, doi: 10.1016/j.geomorph.2015.10.009, 2016.

Guo, X., Cui, P., Marchi, L., and Ge, Y.: Characteristics of rainfall responsible for debris flows in Wenchuan Earthquake area, Environmental Earth Sciences, 76, 596, doi: 10.1007/s12665-017-6940-y, 2017.

Guzzetti, F., Malamud, B. D., Turcotte, D. L., and Reichenbach, P.: Power-law correlations of landslide areas in Central Italy, Earth Planet. Sci. Lett., 195, 169–183, doi: 10.1016/S0012-821X(01)00589-1, 2002.

Guzzetti, F., Peruccacci, S., Rossi, M., and Stark, C. P.: Rainfall thresholds for the initiation of landslides in central and southern Europe, Meteorog. Atmos. Phys., 98, 239–267, doi: 10.1007/s00703-007-0262-7, 2007.

Guzzetti, F., Ardizzone, F., Cardinali, M., Rossi, M., and Valigi, D.: Landslide volumes and landslide mobilization rates in Umbria, central Italy, Earth Planet. Sci. Lett, 279, 222-229, doi: 10.1016/j.epsl.2009.01.005, 2009.

Guzzetti, F., Mondini, A. C., Cardinali, M., Fiorucci, F., Santangelo, M., and Chang, K.-T.: Landslide inventory maps: New tools for an old problem, Earth Sci. Rev., 112 (1-2), 42-66, doi: 10.1016/j.earscirev.2012.02.001, 2012.

Harp, E. L., Keefer, D. K., Sato, H. P., and Yagi, H.: Landslide inventories: the essential part of seismic landslide hazard analyses, Eng. Geol., 122 (1-2), 9-21, doi: 10.1016/j.enggeo.2010.06.013, 2011.

Hovius, N., Meunier, P., and Ching-weei, L.: Prolonged seismically induced erosion and the mass balance of a large earthquake, Earth Planet. Sci. Lett., 304, 347–355, doi: 10.1016/j.epsl.2011.02.005, 2011.

Hu, W., Scaringi, G., Xu, Q., Pei, G., van Asch, T. W. J., and Hicher, P. Y.: Sensitivity of the initiation and runout of flowslides in loose granular deposits to the content of small particles: An insight from flume tests, Eng. Geol., 231, 34-44, doi: 10.1016/j.enggeo.2017.10.001, 2017.

Hu, W., Hicher, P.-Y., Scaringi, G., Xu, Q., van Asch, T. W. J., and Wang, G.: Seismic precursor to instability induced by internal erosion in loose granular slopes, Géotechnique, doi: https://doi.org/10.1680/jgeot.17.P.079, 2018a.

Hu, W., Scaringi, G., Xu, Q., and Huang, R.: Acoustic emissions and micro-seismicity in granular slopes prior to failure and flow-like motion: The potential for early warning, Geophys. Res. Lett., doi: 10.1029/2018GL079724, 2018b.

Hu, W., Scaringi, G., Xu, Q., and Huang, R.: Internal Erosion Controls Failure and Runout of Loose Granular Deposits: Evidence From Flume Tests and Implications for Postseismic Slope Healing, Geophys. Res. Lett., 45 (11), 5518-5527, doi: 10.1029/2018GL078030, 2018c.

Huang, J., Huang, R., Ju, N., Xu, Q., and He, C.: 3D WebGIS platform for debris flow early warning: A case study, Eng. Geol., 197, 57-66, doi: 10.1016/j.enggeo.2015.08.013, 2015.

Huang, R., and Fan, X.: The landslide story, Nature Geosci., 6, 325–326, doi: 10.1038/ngeo1806, 2013.

Hungr, O., Leroueil, S., and Picarelli, L.: The Varnes classification of landslide types, an update, Landslides, 11 (2), 167-194, doi: 10.1007/s10346-013-0436-y, 2014.

Jakob, M., Owen, T., and Simpson, T.: A regional real-time debris flow warning system for the District of North Vancouver, Canada, Landslides, 9, 165–178, doi: 10.1007/s10346-011-0282-8, 2012.

Kargel, J. S., Leonard, G. J., Shugar, D. H. et al.: Geomorphic and geologic controls of geohazards induced by Nepal's 2015 Gorkha earthquake, Science, 351 (6259), aac8353, doi: 10.1126/science.aac8353, 2016.

Keefer, D. K.: Landslides caused by earthquakes, Geological Society of America Bulletin, 95 (4), 406–421, doi: 10.1130/0016-7606(1984)95<406:LCBE>2.0.CO, 1984.

Keefer, D. K.: The importance of earthquake-induced landslides to long-term slope erosion and slope-failure hazards in seismically active regions, Geomorphology, 10, 265–284, doi: 10.1016/0169-555X(94)90021-3, 1994.

Keefer, D. K.: Investigating Landslides Caused by Earthquakes – A Historical Review, Surv. Geophys., 23 (6), 473-510, doi: 10.1023/A:1021274710840, 2002.

Kirschbaum, D., Adler, R., Hong, Y., Kumar, S., Peters-Lidard, C., and Lerner-Lam, A.: Advances in landslide nowcasting: evaluation of a global and regional modeling approach, Environ. Earth Sci., 66, 1683–1696, doi: 10.1007/s12665-011-0990-3, 2012.

Koi, T., Hotta, N., Ishigaki, I., Matuzaki, N., Uchiyama, Y., and Suzuki, M.: Prolonged impact of earthquake-induced landslides on sediment yield in a mountain watershed: The Tanzawa region, Japan, Geomorphology, 101, 692–702, doi: 10.1016/j.geomorph.2008.03.007, 2008.

Larsen, I. J., Montgomery, D. R., Korup, O.: Landslide erosion controlled by hillslope material, Nature Geoscience, 3, 247–251, doi: 10.1038/NGEO776 ,2010.

Li, G., West, A. J., Densmore, A. L., Jing, Z., Zhang, F., Wang, J., Clark, M., and Hilton, R. G.: Earthquakes drive focused denudation along a tectonically active mountain front, Earth Planet. Sci. Lett., 472, 253-265, doi: 10.1016/j.epsl.2017.04.040, 2017.

Lin, C. W., Liu, S. H., Lee, S. Y., and Lu, C. C.: Impacts of the Chi-Chi earthquake on subsequent rainfall-induced landslides in central Taiwan, Eng. Geol., 86, 87-101, doi: 10.1016/j.enggeo.2006.02.010, 2006.

Malamud, B. D., Turcotte, D. L., Guzzetti, F, Reichenbach, P.: Landslide inventories and their statistical properties, Earth Surface Processes Landforms, 29, 687–711, 2014.

Marc, O., and Hovius, N.: Amalgamation in landslide maps: effects and automatic detection, Nat. Hazards Earth Syst. Sci., 15, 723–733, doi: 10.5194/nhess-15-723-2015, 2015.

Marc, O., Hovius, N., Meunier, P., et al.: Transient changes of landslide rates after earthquakes, Geology, 43(10), 883-886, doi: 10.1130/G36961.1, 2015.

Marc, O., Hovius, N., and Meunier, P.: The mass balance of earthquakes and earthquake sequences, Geophys. Res. Lett., 43, 3708–3716, doi: 10.1002/2016GL068333, 2016a.

Marc, O., Hovius, N., Meunier, P., Gorum, T., and Uchida, T.: A seismologically consistent expression for the total area and volume of earthquake-triggered landsliding, J. Geophys. Res.-Earth, 121, 640–663, doi: 10.1002/2015JF003732, 2016b.

Marc, O., Meunier, P., and Hovius, N.: Prediction of the area affected by earthquake-induced landsliding based on seismological parameters, Nat. Hazards Earth Syst. Sci., 17, 1159-1175, doi: 10.5194/nhess-17-1159-2017, 2017.

Meunier, P., Hovius, N., and Haines, J. A.: Topographic site effects and the location of earthquake induced landslides, Earth Planet. Sci. Lett. 275, 221–232, doi: 10.1016/j.epsl.2008.07.020, 2008.

Nikolopoulos, E. I., Crema, S., Marchi, L., Marra, F., Guzzetti, F., and Borga, M.: Impact of uncertainty in rainfall estimation on the identification of rainfall thresholds for debris flow occurrence, Geomorphology, 221, 286–297, doi: 10.1016/j.geomorph.2014.06.015, 2014..

Panziera, L., Germann, U., Gabella, M., and Mandapaka, P. V.: NORA—Nowcasting of Orographic Rainfall by means of Analogues, Q. J. R. Meteorol. Soc., 137, 2106–2123, doi: 10.1002/qj.878, 2011.

Parker, R. N., Densmore, A. L., Rosser, N. J., De Michele, M., Li, Y., Huang, R., Whadcoat, S., and Petley, D. N.: Mass wasting triggered by the 2008 Wenchuan earthquake is greater than orogenic growth, Nature Geosci. 4, 449–452, doi: 10.1038/ngeo1154, 2011.

Parker, R. N., Hancox, G. T., Petley, D. N., et al.: Spatial distributions of earthquake-induced landslides and hillslope preconditioning in the northwest South Island, New Zealand, Earth Surf. Dyn., 3, 501-525, doi: 10.5194/esurf-3-501-2015, 2015.

Pawłuszek, K., Borkowski, A., and Tarolli, P.: Towards the optimal pixel size of DEM for automatic mapping of landslide areas. The International Archives of the Photogrammetry, Remote Sensing and Spatial Information Sciences, Vol. XLII-

1/W1, 2017 ISPRS Hannover Workshop: HRIGI 17 – CMRT 17 – ISA 17 – EuroCOW 17, 6–9 June 2017, Hannover, Germany. https://doi.org/10.5194/isprs-archives-XLII-1-W1-83-2017, 2017.

Rodriguez, C. E., Bommer, J. J., Chandler, R. J.: Earthquake-induced landslides: 1980–1997. Soil Dynamics and Earthquake Engineering, 18, 325–346, doi: 10.1016/S0267-7261(99)00012-3, 1999.

Rossi, M., Kirschbaum, D., Luciani, S., Mondini, A. C., and Guzzetti, F.: TRMM satellite rainfall estimates for landslide early warning in Italy: preliminary results. Proceedings of SPIE — The International Society for Optical Engineering, 8523, art. no. 85230D, 2012.

Qi, S., Xu, Q., Lan, H., Zhang, B., and Liu, J.: Spatial distribution analysis of landslides triggered by 2008.5.12 Wenchuan Earthquake, China, Eng. Geol., 116, 95-108, doi: 10.1016/j.enggeo.2010.07.011, 2010.

Santangelo, M., Marchesini, I., and Bucci, M.: An approach to reduce mapping errors in the production of landslide inventory maps, Nat. Hazards Earth Syst. Sci., 15, 2111–2126, doi: 10.5194/nhess-15-2111-2015, 2015.

Scaringi, G., Fan, X., Xu, Q., Liu, C., Ouyang, C., Domènech, G., Yang, F., and Dai, L.: Some considerations on the use of numerical methods to simulate past landslides and possible new failures: the case of the recent Xinmo landslide (Sichuan, China), Landslides, 15 (7), 1359-1375, doi: 10.1007/s10346-018-0953-9, 2018.

Schmitt, R. G., Tanyas, H., Nowicki Jessee, M. A., et al.: An open repository of earthquake-triggered ground-failure inventories: U.S. Geological Survey data release collection, doi: 10.5066/F7H70DB4, 2017.

Shieh, C. L., Chen, Y. S., Tsai, Y. J., and Wu, J. H.: Variability in rainfall threshold for debris flow after the Chi-Chi earthquake in central Taiwan, China, Int. J. Sediment. Res., 24, 177–188, doi: 10.1016/S1001-6279(09)60025-1, 2009.

Smith, R. B., Jiang, Q., Fearon, M. G., Tabary, P., Dorninger, M., Doyle, J. D., and Benoit, R.: Orographic precipitation and air mass transformation: an Alpine example, Q. J. R. Meteorol. Soc., 129, 433–454, doi: 10.1256/qj.01.212, 2003.

Stoffel, M., Bollschweiler, M., and Beniston, M.: Rainfall characteristics for periglacial debris flows in the Swiss Alps: past incidences—potential future evolutions, Clim. Chang., 105, 263–280, doi: 10.1007/s10584-011-0036-6, 2011.

Takahashi, T.: Debris flow. Monograph of IAHR. AA Balkema, Rotterdam, 1991.

Tang, C., Zhu, J., Li, W. L., and Liang, J. T.: Rainfall-triggered debris flows following the Wenchuan earthquake, Bull. Eng. Geol. Environ., 68 (2), 187-194, doi: 10.1007/s10064-009-0201-6, 2009.

Tang, C., Zhu, J., Ding, J., et al.: Catastrophic debris flows triggered by a 14 August 2010 rainfall at the epicenter of the Wenchuan earthquake, Landslides, 8, 485–497, doi: 10.1007/s10346-011-0269-5, 2011.

Tang, C., van Asch, T.W J., Chang, M., Chen, G. Q., Zhao, X. H., and Huang, X. C.: Catastrophic debris flows on 13 august 2010 in the Qingping area, southwestern china: the combined effects of a strong earthquake and subsequent rainstorms, Geomorphology 139, 559-576, doi: 10.1016/j.geomorph.2011.12.021, 2012.

Tang, C., van Westen, C. J., Tanyas, H., and Jetten, V. G.: Analysing post-earthquake landslide activity using multi-temporal landslide inventories near the epicentral area of the 2008 Wenchuan earthquake, Nat. Hazards Earth Syst. Sci. 16, 2641-2655, doi: 10.5194/nhess-16-2641-2016, 2016.

Tang, R., Fan, X., Scaringi, G., Xu, Q., van Westen, C. J., Ren, J., Havenith, H. B.: Distinctive controls on the distribution of river-damming and non-damming landslides induced by the 2008 Wenchuan earthquake, Bull. Eng. Geol. Environ., doi: 10.1007/s10064-018-1381-8, 2018.

Tanyas, H., van Westen, C. J., Allstadt, K. E., et al.: Presentation and Analysis of a Worldwide Database of Earthquake-Induced Landslide Inventories, J. Geophys. Res.-Earth, 122 (10), 1991-2015, doi: 10.1002/2017JF004236, 2017.

Turcotte, D. L., Malamud, B. D., Guzzetti, F., Reichenbach, P.: Self-organization, the cascade model, and natural hazards. Proc Natl Acad Sci U S A 19,:2530–2537, 2002.

van Westen, C.J., Seijmonsbergen, A.C., Mantovani, F.: Comparing landslide hazard maps, Natural Hazards, 20, 137–158, 1999.

van Westen, C. J., van Asch, T. W. J, and Soeters, R.: Landslide hazard and risk zonation—why is it still so difficult?, Bull. Eng. Geol. Environ., 65, 167–184, doi: 10.1007/s10064-005-0023-0, 2006.

Wang, G., Huang, R., Lourenço, D. N., and Kamai, T.: A large landslide triggered by the 2008 Wenchuan (M8.0) earthquake in Donghekou area: Phenomena and mechanisms, Eng. Geol., 182, 148-157, doi: 10.1016/j.enggeo.2014.07.013, 2014.

Wang, J., Jin, Z., Hilton, R. G., et al.: Controls on fluvial evacuation of sediment from earthquake-triggered landslides, Geology, 43(2), 115-118, doi: 10.1130/G36157.1, 2015.

Wang, W., Godard, W., Liu-Zeng, J., et al.: Perturbation of fluvial sediments fluxes following the 2008 Wenchuan earthquake, Earth Surface Processes and Landforms, 42 (15), 2611-2622, doi: 10.1002/esp.4210, 2017.

Xu, C., Xu, X., Yao, X., and Dai, F.: Three (nearly) complete inventories of landslides triggered by the May 12, 2008 Wenchuan Mw 7.9 earthquake of China and their spatial distribution statistical analysis, Landslides, 11, 441–461, doi: 10.1007/s10346-013-0404-6, 2014.

Xu, C., Xu, X., Lingling, S., et al.: Optimized volume models of earthquake-triggered landslides, Sci. Rep., 6, 29797, doi: 10.1038/srep29797, 2016.

Xu, Q., Zhang, S., Li, W. L., and Van Asch, T. W. J.: The 13 August 2010 catastrophic debris flows after the 2008 Wenchuan earthquake, China, Nat. Hazards Earth Syst. Sci., 12, 201–216, doi: 10.5194/nhess-12-201-2012, 2012.

Yan, Y., Cui, P., Guo, X. J., Ge, Y. G.: Trace projection transformation: a new method for measurement of debris flow surface velocity fields. Front. Earth Sci., 10 (4), 761–771, doi: 10.1007/s11707-015-0576-6.

Yang, W., Qi, W., Wang, M., et al.: Spatial and temporal analyses of post-seismic landslide changes near the epicentre of the Wenchuan earthquake, Geomorphology, 276, 8-15, doi: 10.1016/j.geomorph.2016.10.010, 2016.

Yang, W., Qi, W., and Zhou, J.: Decreased post-seismic landslides linked to vegetation recovery after the 2008 Wenchuan earthquake, Ecol. Eng., 89, 438-444, doi: 10.1016/j.ecolind.2017.12.006, 2018.

Yu, B., Ma, Y., and Wu, Y.: Investigation and study of debris flow disasters in Wenjiagou, Qingping Township, Mianzhu City, Sichuan Province, Journal of Engineering Geology, 18 (6), 827-836, 2010 (in Chinese).

Yu, B., Wu, Y. F., and Chu, S. M.: Preliminary study of the effect of earthquakes on the rainfall threshold of debris flows. Eng. Geol., 182, 130–135, doi: 10.1016/j.enggeo.2014.04.007, 2014.

Zhang, S., and Zhang, L. M.: Impact of the 2008 Wenchuan earthquake in China on subsequent long-term debris flow activities in the epicentral area, Geomorphology, 276, 86–103, doi: 10.1016/j.geomorph.2016.10.009, 2017.

Zhang S, Zhang L. M., Chen H. X.: Relationships among three repeated large-scale debris flows at Pubugou Ravine in the Wenchuan earthquake zone, Can. Geotech. J., 51, 951–965, doi: 10.1139/cgj-2013-0368, 2014.

Zhang, S., Zhang, L., Lacasse, S., and Nadim, F.: Evolution of Mass Movements near Epicentre of Wenchuan Earthquake, the First Eight Years, Sci. Rep., 6, 36154, doi: 10.1038/srep36154, 2016.